Gasdermin D permeabilization of mitochondrial inner and outer membranes accelerates and enhances pyroptosis

Rui Miao[1,2,15]*, Cong Jiang[3,4,15], Winston Y. Chang[1,2,15], Haiwei Zhang[1,2], Jinsu An[1,2], Felicia Ho[1,2], Pengcheng Chen[4], Han Zhang[3,4], Caroline Junqueira[1,2,5], Dulguun Amgalan[6], Felix G. Liang[6], Junbing Zhang[7], Charles L. Evavold[8], Iva Hafner-Bratkovič[9,10], Zhibin Zhang[1,2,11], Pietro Fontana[1,12], Shiyu Xia[1,12], Markus Waldeck-Weiermair[13], Youdong Pan[14], Thomas Michel[13], Liron Bar-Peled[7], Hao Wu[1,12], Jonathan C. Kagan[9], Richard N. Kitsis[6], Peng Zhang[3]*, Xing Liu[4]* and Judy Lieberman[1,2,16]*

[1]Program in Cellular and Molecular Medicine, Boston Children's Hospital, Boston, MA 02115, USA
[2]Department of Pediatrics, Harvard Medical School, Boston, MA 02115, USA
[3]Department of Thoracic Surgery, Shanghai Pulmonary Hospital, School of Medicine, Tongji University, Shanghai, 200433, China
[4]Key Laboratory of RNA Science and Engineering, Shanghai Institute of Immunity and Infection, Chinese Academy of Sciences, Shanghai, 200031, China
[5]Instituto René Rachou, Fundação Oswaldo Cruz, Belo Horizonte, MG 30190-009 Brazil
[6]Departments of Medicine and Cell Biology, Wilf Family Cardiovascular Research Institute, Albert Einstein College of Medicine, Bronx, NY 10461, USA
[7]Center for Cancer Research, Massachusetts General Hospital and Department of Medicine, Harvard Medical School, Boston, MA 02129, USA
[8]Ragon Institute of MGH, MIT and Harvard, Cambridge, MA 02139, USA
[9]Division of Gastroenterology, Boston Children's Hospital and Harvard Medical School, Boston, MA 02115, USA
[10]Department of Synthetic Biology and Immunology, National Institute of Chemistry and EN-FIST Centre of Excellence, 1000 Ljubljana, Slovenia
[11]Department of Immunology, The University of Texas MD Anderson Cancer Center, Houston, TX 77030, USA
[12]Department of Biological Chemistry and Molecular Pharmacology, Harvard Medical School, Boston, MA 02115, USA
[13]Brigham and Women's Hospital, Department of Medicine, Cardiovascular Division, Harvard Medical School, Boston, MA 02115, USA
[14]Department of Dermatology and Harvard Skin Disease Research Center, Brigham and Women's Hospital, Harvard Medical School, Boston, MA 02115, USA
[15]These authors contributed equally
[16]Lead Contact
* Correspondence: rui.miao@childrens.harvard.edu (R.M.), zhangpeng1121@tongji.edu.cn (P.Z.), xingliu@ips.ac.cn (X.L.), judy.lieberman@childrens.harvard.edu (J.L.)

Summary
Gasdermin D (GSDMD)-activated inflammatory cell death (pyroptosis) causes mitochondrial damage, but its underlying mechanism and functional consequences are largely unknown. Here, we show that the N-terminal pore-forming GSDMD fragment (GSDMD-NT) rapidly damaged both inner and outer mitochondrial membranes leading to reduced mitochondrial numbers, mitophagy, ROS, loss of transmembrane potential, attenuated oxidative phosphorylation and release of mitochondrial proteins and DNA from the matrix and intermembrane space. Mitochondrial damage occurred as soon as GSDMD was cleaved prior to plasma membrane damage. Mitochondrial damage was independent of the B-cell lymphoma 2 family and depended on GSDMD-NT binding to cardiolipin. Canonical and noncanonical inflammasome activation of mitochondrial damage, pyroptosis and inflammatory cytokine release were suppressed by genetic ablation of cardiolipin synthase (*Crls1*) or the scramblase (*Plscr3*) that transfers cardiolipin to the outer mitochondrial membrane. PLSCR3 deficiency in a tumor compromised pyroptosis-triggered anti-tumor immunity. Thus, mitochondrial damage plays a critical role in pyroptosis.

Key words Pyroptosis, GSDMD, Mitochondria, Cardiolipin, CRLS1, PLSCR3, IL-1

Introduction

When immune cells and barrier epithelia sense invasive pathogens and danger signals, they assemble cytosolic pattern recognition receptors, called inflammasomes, which recruit and activate inflammatory caspases (caspase-1, 4, 5, 11)[1]. Caspase-1 is activated by canonical inflammasomes (NOD-like receptors, pyrin and AIM2-like receptors). Cytosolic lipopolysaccharide (LPS) from invasive gram-negative bacteria and endogenous oxidized phospholipids bind and activate human caspases-4 and -5 and mouse caspase-11 to assemble the noncanonical inflammasome[1,2]. Gasdermin D (GSDMD), a substrate of all the inflammatory caspases, executes inflammasome-induced cell death, called pyroptosis[3,4]. Proteolytic cleavage liberates an N-terminal (NT) pore-forming fragment from the autoinhibitory C-terminus[5-7]. GSDMD-NT binds to acidic phospholipids on the inner leaflet of the plasma membrane and oligomerizes to form membrane pores that disrupt the cell membrane and release inflammatory cytokines and cellular alarmins, including interleukin-1 (IL-1) family cytokines[8-11].

Mitochondria are central hubs that control cell fate and immune responses[12-14]. During apoptosis, the outer mitochondrial membrane (OMM) is permeabilized by activating pro-apoptotic bcl-2 family members, BAX and BAK, to release apoptogenic factors, including cytochrome c, from the mitochondrial intermembrane space (IMS) to the cytosol[15]. Mitochondrial outer membrane permeabilization (MOMP) triggers formation of the apoptosome, which activates caspase-9 to cleave and activate caspase-3, providing a potent feed forward mechanism to amplify cell death, called the “point of no return”[16]. Late in apoptosis, the mitochondrial permeability transition (mPT) disrupts the inner mitochondrial membrane, causing persistent mitochondrial depolarization[17]. Mitochondrial ROS and loss of transmembrane potential are also generated by caspase-independent programmed cell death, including granzyme-mediated killing, necroptosis and ferroptosis, which mostly do not trigger MOMP[18-20].

Mitochondria are damaged early in GSDMD- and GSDME-mediated pyroptosis[21,22] . Mitochondrial ROS, transmembrane potential loss, cytochrome c and mitochondrial DNA (mtDNA) release to the cytosol have previously been described[23-26]. While mitochondrial ROS facilitates pyroptosis[27,28], it is unclear whether its role is critical. Moreover, mechanisms behind pyroptotic mitochondrial damage and how much it contributes to cell death are unclear.

The first step in forming gasdermin (GSDM) pores is GSDM-NT binding to acidic phospholipids. GSDM-NTs bind more strongly to cardiolipin, found on mitochondrial and bacterial membranes, than to plasma membrane acidic phospholipids[5,6]. Basally cardiolipin is located almost exclusively on the matrix side of the IMM and only small amounts (~3-5%) are found in the OMM[29,30], where it might be accessible to cytosolic GSDMs. Cardiolipin is synthesized by cardiolipin synthase 1 (CRLS1) in the matrix and can be flipped from the IMM inner leaflet to the IMM outer leaflet by phospholipid scramblase-3 (PLSCR3) and from there to both leaflets of the OMM[31,32]. OMM cardiolipin is an important sign of mitochondrial damage, which triggers mitophagy to remove damaged mitochondria[29]. Mitochondrial toxins that induce mitochondrial ROS and/or loss of transmembrane potential cause cardiolipin transfer to the OMM, where it could anchor GSDM-NT binding[33].

Here we show that GSDMD-NT triggers a mitochondrial cell death pathway. GSDMD-NT disrupts both mitochondrial membranes early in pyroptosis, leading to mitochondrial damage prior to plasma membrane permeabilization. Mitochondrial damage during pyroptosis depends on OMM cardiolipin since it is virtually abrogated by genetic ablation of either *Crls1* or *Plscr3*. It occurs independently of BAX, BAK and mPT pore (mPTP). It disrupts mitochondrial morphology and respiration and induces mitophagy, reducing mitochondrial numbers. Mitochondrial damage depends on GSDMD permeabilization of both mitochondrial membranes, releasing contents of the

IMS and matrix, including mtDNA. Release of the IMS exoRNase PNPT1 leads to global mRNA decay, enhancing pyroptosis, as previously described in apoptosis[34]. Moreover, mitochondrial damage is critical for pyroptotic cell death and inflammation.

Results

Mitochondria are damaged during pyroptosis

To dissect the role of mitochondria in pyroptosis, mitochondrial integrity and membrane potential were assessed in LPS+nigericin-treated THP-1 cells stained with mitochondrial transmembrane potential-sensitive MitoTracker deep red (MTDR) and insensitive MitoTracker green (MTG) and the potentiometric dye, tetramethylrhodamine methyl ester (TMRM) (Figure 1A and 1B). MTDR and TMRM fluorescence were markedly diminished in SYTOX or propidium iodide (PI)-positive pyroptotic cells compared to adjacent SYTOX or PI-negative live cells, while MTG staining persisted, indicating that mitochondria depolarize during pyroptosis. The extracellular acidification rate (ECAR) and oxygen consumption rate (OCR) were measured to assess glycolysis and OXPHOS, respectively, in mitochondrial metabolism (Figure S1A-C). Because LPS priming on its own shifted metabolism from OXPHOS to glycolysis (Figure S1A) as previously reported[35,36], pyroptosis was stimulated using nigericin without LPS (Figure S1C). Nigericin on its own rapidly increased ECAR and suppressed mitochondrial respiration, indicating that mitochondrial OXPHOS was attenuated during pyroptosis (Figure S1B). Transmission electron microscopy (TEM) of LPS-primed THP-1 cells before and after adding nigericin to trigger pyroptosis showed that mitochondrial morphology changed – before nigericin, mitochondria were typical ovoid-shaped, double membrane-bound vesicles with internal cristae, but after adding nigericin, mitochondria had shrunk and rounded up with a ~2-fold reduced mean length (Figure 1C and 1D). Autophagosomes containing damaged mitochondria were observed within 15 min of adding nigericin. After one hour, ~60% of mitochondria had whirled or absent cristae and/or broken IMM and OMM and mitochondrial numbers decreased ~2-fold. Thus, mitochondria are profoundly damaged early after triggering pyroptosis.

To assess the role and kinetics of GSDMD pores in mitochondrial damage, nigericin-treated THP-1 culture medium and mitochondrial and cytosolic fractions were analyzed by immunoblot for caspase-1, GSDMD and pro-IL-1β cleavage, GSDMD-NT binding to mitochondria and cytosolic release and secretion of mitochondrial contents (IMS cytochrome c, matrix ACO2 and mtDNA) (Figure 1E-G). The mitochondrial fraction did not contain detectable nuclear (Lamin B1), lysosomal (LAMP1), endosomal (EEA1) or endoplasmic reticulum (calnexin) markers (Figure S1D). Caspase-1, GSDMD and IL-1β were cleaved within 7.5 min. GSDMD-NT, but not full-length GSDMD (GSDMD-FL), was also detected in the mitochondrial fraction at 7.5 min, indicating that GSDMD-NT binds to mitochondria soon after it is generated. Within 7.5 and 15 min of adding nigericin, mtDNA and soluble cytochrome c and ACO2, but not IMM-associated COX IV, were detected in the cytosol, indicating rapid disruption of both mitochondrial membranes, consistent with rapid GSDMD-NT pore formation. By contrast, IL-1β, cytochrome c and ACO2 were not detected in culture supernatants until 30 min after adding nigericin, indicating delayed plasma membrane permeabilization. These data suggest that GSDMD-NT permeabilizes both OMM and IMM before the plasma membrane. Because cytosolic mtDNA could activate the AIM2 inflammasome to amplify pyroptosis[37], AIM2 speck formation in iBMDMs was examined after LPS+nigericin or LPS transfection, which do not directly activate AIM2, or poly(dA:dT) transfection to directly activate AIM2 (Figure S1E). AIM2 specks were similarly detected in poly(dA:dT) and LPS-transfected iBMDMs, suggesting that mtDNA release secondarily activated AIM2. AIM2 specks were not detected in LPS+nigericin-treated cells, perhaps because ASC may have been depleted by recruitment to NLRP3.

Mitochondrial dysfunction occurs early in pyroptosis and is required for pyroptosis

Mitochondrial membrane potential (TMRM intensity), cellular ROS production (DCFDA intensity) and plasma membrane permeabilization (SYTOX green uptake) were also assessed in LPS+nigericin-treated THP-1 by plate reader (Figure 2A). DCFDA increased and TMRM decreased before cells took up SYTOX green, confirming that mitochondrial dysfunction precedes cell death. This was corroborated by flow cytometry of MitoSOX (mitochondrial ROS), DiIC1(5) (mitochondrial membrane potential) and SYTOX green uptake (Figure 2B). Significant changes in MitoSOX and DiIC1(5) were detected ~10 min before SYTOX green uptake.

To test the importance of mitochondrial damage in pyroptosis, immortalized mouse bone marrow-derived macrophages (iBMDMs) were treated with ethidium bromide (EB) to generate mitochondria-deficient ρ° cells[38] (Figure 2C). EB-untreated and treated iBMDMs similarly upregulated the expression of pro-inflammatory cytokines (IL-1β, IL-6, TNF-α), NLRP3, ASC and pro-caspase-11 after LPS-priming and similarly activated caspase-1 and GSDMD cleavage after LPS+nigericin (Figure S1F-S1H). However, ρ° iBMDMs were highly resistant to both canonical (LPS+nigericin) and non-canonical (transfected LPS) inflammasome-mediated pyroptosis by CellTiterGlo assay (Figure 2D and 2E), suggesting a critical role of mitochondria in pyroptotic cell death.

We next investigated whether mitochondrial ROS contributes to pyroptosis in iBMDMs by scavenging mitochondrial ROS with MitoTEMPO. SYTOX green uptake and LDH release induced by LPS+nigericin or LPS or dA:dT transfection was blunted in MitoTEMPO-treated iBMDMs (Figure 2F-2I), even though nigericin-induced caspase-1 and GSDMD cleavage were not affected by MitoTEMPO (Figure S1I). To confirm the role of ROS in pyroptosis, a chemogenetic system was used to locally manipulate intracellular redox status by expressing a yeast D-amino acid oxidase (DAAO) (which converts D-amino acids, but not endogenous L-amino acids, to alpha-keto acids to produce H_2O_2)[39], tagged with nuclear export or localization sequences[40] and a ratiometric H_2O_2-sensitive fluorescent biosensor HyPer7[41] (Figure 2J-L). Addition of D-alanine, but not L-alanine, to cells expressing cytosolic Hyper7-DAAO increased cytosolic H_2O_2 and pyroptosis. In contrast, D-alanine did not enhance pyroptosis in iBMDMs expressing nuclear HyPer7-DAAO. Thus, cytosolic ROS amplifies canonical and noncanonical inflammasome-mediated pyroptosis, as previously described[24,28,42].

GSDMD-NT translocates to and damages mitochondria before plasma membrane disruption

To determine in live cells whether GSDMD-NT binds to and mediates mitochondrial dysfunction, we imaged iBMDMs expressing doxycycline (DOX)-inducible I105N GSDMD-NT fused at its C-terminus to BFP (GSDMD-NT-BFP)[28]. The I105N mutation slows pyroptosis, enabling better detection of dying cells[7]. GSDMD-NT-BFP was detected 4-8 h after DOX induction. The dynamics of GSDMD-NT localization, plasma membrane permeabilization (PI or SYTOX uptake) and mitochondrial damage (MitoTracker, TMRM and MitoSOX) was followed beginning 6 h after adding DOX by live-cell confocal imaging (Figures 3A and 3B, S2A and S2B). Pyroptotic changes were synchronized by defining time 0 for each cell at the first detection of dye uptake (plasma membrane damage). After DOX, both MitoTracker and TMRM intensities decreased in GSDMD-NT-BFP-expressing cells that eventually died, as assessed by PI or SYTOX uptake (Figure 3A and 3B), while mitochondrial dye intensities and PI uptake were unaltered in cells expressing FL-GSDMD-BFP (Figure S2C-F). GSDMD-NT-BFP localized with mitochondrial dyes at least 50 min before plasma membrane permeabilization (Figure 3A and 3B), confirming early GSDMD-NT targeting to mitochondria. MitoTracker and TMRM intensities gradually decreased while the MitoSOX signal increased prior to PI or SYTOX uptake. All the mitochondrial markers eventually dissipated, suggesting mitochondrial dissolution. Late in pyroptosis after the plasma membrane had been

permeabilized, MitoSOX Red, released from damaged mitochondria, stained the nucleus, as previously noted[43].

Mitochondrial ROS and loss of transmembrane potential also occurred early in THP-1 treated with LPS+nigericin, even though cell death occurred more rapidly than after ectopic expression of GSDMD-NT-BFP (Figure S2G and S2H). Thus, GSDMD-NT mitochondrial binding and dysfunction precedes plasma membrane permeabilization. To corroborate the colocalization of GSDMD-NT with mitochondria, we expressed Flag-tagged GSDMD-FL or -NT in HEK293T. Eighteen hours after transfection, when ~30% of the cells expressing GSDMD-NT had died, localization of GSDMD-FL and GSDMD-NT were analyzed by confocal microscopy (Figure 3C), Structured Illumination Microscopy (SIM) (Figure 3D), and immune-electron microscopy (EM, Figure 3E). In the fluorescence microscopy images, ectopic GSDMD-NT, but not GSDMD-FL, largely colocalized with and formed puncta on mitochondria (Figure 3C and 3D). Similarly, in immuno-EM, anti-Flag-conjugated gold particles were enriched in mitochondria 18 h after transfection only in GSDMD-NT-expressing cells (Figure 3E). Few gold particles were detected on the plasma membrane at this early time, confirming that GSDMD-NT goes to mitochondria before the plasma membrane (Figure S2I).

To confirm the importance of GSDMD in mitochondrial damage, MTDR and TMRM, dye uptake, mitochondrial ultrastructure and mitochondrial release of cytochrome c, ACO2 and mtDNA were compared in LPS+nigericin-treated WT and *Gsdmd*$^{-/-}$ iBMDMs (Figure S3A-F). Mitochondria were preserved after adding nigericin to *Gsdmd*$^{-/-}$, compared to WT, iBMDMs, implicating GSDMD in pyroptotic mitochondrial damage. Consistent with a direct role of GSDMD in mitochondrial damage, mitochondrial damage from LPS or poly(dA:dT) transfection was not inhibited by the NLRP3 inhibitor MCC950 (Figure S3G and S3H).

Pyroptotic mitochondrial damage is independent of BAX, BAK and the mPTP

During apoptosis, pro-apoptotic BCL-2 family proteins (BAX, BAK) form OMM pores, leading to MOMP, but leave the IMM intact. To determine whether BAX or BAX are involved in pyroptosis, SYTOX green uptake was compared in WT, *BAX*$^{-/-}$, *BAK*$^{-/-}$ and *BAK*$^{-/-}$ *BAX*$^{-/-}$ HEK293T cells expressing GSDMD-FL or GSDMD-NT (Figure S3I and S3J). GSDMD-FL expression did not cause cell death in any of the cells, as expected, while GSDMD-NT expression similarly induced pyroptosis in BAX and/or BAK deficient as in WT HEK293T, suggesting that BAX and BAK are not involved in GSDMD-mediated mitochondrial damage. To determine whether mPTP is involved, iBMDMs were pretreated with inhibitors of key mPTP components (the adenine nucleotide translocator 1 (ANT1), cyclophilin D (CYPD), the voltage-dependent anion channel (VDAC), and mitochondrial phosphate carrier (PiC)) and LPS+nigericin-induced pyroptosis was assessed by TMRM staining and SYTOX green uptake (Figure S3K). Mitochondrial depolarization and cell death were only slightly affected by mPTP inhibitors, suggesting that mPTP does not strongly contribute to pyroptotic mitochondrial damage.

GSDMD-NT damages isolated mitochondria *in vitro*

To determine whether GSDMD-NT on its own binds to and damages mitochondrial membranes, isolated mitochondria were treated with recombinant GSDMD and caspase-11 to generate active GSDMD-NT, and mitochondrial permeability was assessed by immunoblotting for released mitochondrial proteins (Figure 4A and 4B). Soluble mitochondrial matrix protein (ACO2) and IMS proteins (cytochrome c and HtrA2), but not membrane-bound COX IV, were released from mitochondria within 5 min of adding both caspase-11 and GSDMD, but not after adding them separately. As expected, the pan-caspase inhibitor z-VAD-FMK inhibited release. Cytochrome c

and HtrA2, but not ACO2, were released after adding t-Bid, which triggerred MOMP without disrupting the IMM in apoptosis. mtDNA was also released when mitochondria were incubated with both GSDMD and caspase-11, but not with either alone or with t-Bid (Figure 4C). GSDMD and caspase-11 treatment of isolated mitochondria also significantly increased ROS and reduced membrane potential by MitoSOX Red and DiIC1(5) staining, respectively (Figure 4D and 4E). Thus, GSDMD-NT directly permeabilizes both OMM and IMM without requiring other factors.

Disulfiram (DSF) inhibits GSDMD pore formation without interfering with GSDMD cleavage or GSDMD-NT binding to membranes[44]. To corroborate the role of GSDMD-NT pores in mitochondrial membrane damage, isolated mitochondria were preincubated with DSF before adding GSDMD and caspase-11 (Figure 4F and 4G). DSF blocked mitochondrial release of both cytochrome c and mtDNA, confirming that GSDMD-NT pores permeabilize mitochondria.

OMM cardiolipin is required for GSDMD-NT-mediated mitochondrial damage

Because GSDMD-NT has high affinity for cardiolipin[5,6] and mitochondrial membranes do not contain other known GSDMD-NT-binding lipids, we hypothesized that mitochondrial damage depends on mitochondrial cardiolipin. Cardiolipin is synthesized by CRLS1 and externalized to the OMM by PLSCR3 (Figure 5A)[33]. To investigate whether OMM cardiolipin is required for GSDMD-NT-mediated mitochondrial damage, *Crls1* and *Plscr3* were genetically ablated in iBMDMs (Figure S4A and S4B). GSDMD containing an internal mNeonGreen tag just before the caspase cleavage site was expressed in *Plscr3*$^{-/-}$ and *Crls1*$^{-/-}$ iBMDMs[45]. In LPS+nigericin-treated *Crls1*$^{-/-}$ and *Plscr3*$^{-/-}$ iBMDMs, GSDMD-NT was not recruited to mitochondria (Figure 5B) and mitochondrial integrity and membrane potential (Figure 5C), mitochondrial number and mean length, and damaged mitochondria percentage (Figure 5D and 5E) were restored almost to what they were in untreated WT iBMDMs. Moreover, mitochondrial ROS (Figure S4C), and cytosolic release of cytochrome *c* and mtDNA (Figure 5F-5I) were blocked. Consistently, isolated mitochondria from *Crls1*$^{-/-}$ and *Plscr3*$^{-/-}$ iBMDMs treated with GSDMD and caspase-11 did not release cytochrome c, HtrA2 or mtDNA (Figure S4D and S4E). Taken together, these data indicate that OMM cardiolipin mediates GSDMD-dependent mitochondrial damage.

OMM cardiolipin promotes pyroptosis, IL-1β release, and anti-tumor immunity

To evaluate the importance of OMM cardiolipin and mitochondrial damage in pyroptosis, LPS+nigericin-treated *Plscr3*$^{-/-}$, *Crls1*$^{-/-}$ and WT iBMDMs were compared (Figure 5J-5M, Figure S4F-J). Events upstream of membrane damage, including ASC speck formation, caspase-1 and GSDMD cleavage, and GSDMD oligomerization, were not affected by *Plscr3* and *Crls1* genetic ablation (Figure S4F-H), but GSDMD targeting to the plasma membrane, PI uptake and LDH release were reduced by >2-fold in *Plscr3*$^{-/-}$ and *Crls1*$^{-/-}$, compared to WT, iBMDMs (Figure S4I, Figure 5J-5M). Importantly, IL-1β release was abrogated by genetic ablation of *Plscr3* or *Crls1* (Figure S4J). Similar results were obtained when pyroptosis was induced by *Salmonella* (Figure S4K-N) or in iBMDMs ectopically expressing I105N GSDMD-NT (Figure S4O-Q).

To investigate the immunological role of mitochondrial damage *in vivo, Plscr3* was genetically ablated in J774, a mouse macrophage tumor cell line[46] (Figure 5N). Compared with control sgRNA-transduced WT cells, LPS+nigericin-stimulated pyroptosis was significantly reduced in *Plscr3*$^{-/-}$ J774 cells (Figure 5O). Pyroptosis causes immunogenic cell death (ICD), while the cytotoxic drug mitomycin C (MMC) does not[47,48]. To assess the importance of mitochondrial damage in pyroptotic ICD, LPS+nigericin- or MMC-treated control or *Plscr3*$^{-/-}$ J774 were mixed with WT J774 and subcutaneously injected into mice. Tumors exposed to nigericin-treated *Plscr3*$^{-/-}$ J774 grew faster

than those exposed to nigericin-treated WT J774, while PLSCR3 deficiency in MMC-treated J774 cells did not affect tumor growth (Figure 5P). Consistent with the immunogenicity of pyroptosis, tumors exposed to MMC-treated J774 grew much faster than those exposed to LPS+nigericin-treated J774. These data indicate that mitochondrial damage promotes pyroptosis-induced anti-tumor immunity *in vivo*.

CRLS1 and PLSCR3 activity and mitochondrial localization are required to enhance pyroptosis

To confirm the importance of OMM cardiolipin in pyroptosis, we expressed WT PLSCR3 or PLSCR3 in which Cys159-161-163-164-166 were mutated to Ala (PLSCR3-5A), which causes PLSCR3-5A mislocalization to the nucleus[49], in *Plscr3*$^{-/-}$ iBMDMs (Figure S5A). WT PLSCR3, but not PLSCR3-5A, rescued nigericin- or *Salmonella*-induced pyroptosis, indicating that PLSCR3 mitochondrial localization is required for promoting pyroptosis (Figure S5B). Consistently, genetic ablation of the plasma membrane scramblase *Plscr1* did not affect nigericin- or *Salmonella*-induced pyroptosis (Figure S5C). To investigate whether PLSCR3 scramblase activity is needed to promote pyroptosis, *Plscr3*$^{-/-}$ iBMDMs were rescued with WT *Plscr3* or *Plscr3* encoding a mutation of Phe259, which disrupts PLSCR3 activity[32]. WT, but not F259V, PLSCR3 restored LPS+nigericin- or *Salmonella*-induced PI uptake and LDH release (Figure S5D-G). Similarly, expression of WT CLRS1, but not D170A CRLS1, which disrupts cardiolipin synthesis[31,50], rescued LPS+nigericin- or *Salmonella*-induced pyroptosis in *Crls1*$^{-/-}$ iBMDMs (Figure S5H-K). As expected, GSDMD and IL-1β cleavage after these inflammasome activators was not affected by KO or mutation of *Plscr3* or *Crls1* (Figure S5E, S5G, S5I and S5K). Thus, active PLSCR3 and CRLS1 are required to promote pyroptosis.

Because mitochondrial ROS enhanced pyroptosis (Figure 2F-L), we asked whether mitochondrial ROS on its own could rescue defective pyroptosis in *Plscr3*$^{-/-}$ and *Crls1*$^{-/-}$ cells. LPS-primed *Plscr3*$^{-/-}$ and *Crls1*$^{-/-}$ iBMDMs were pretreated with the complex I inhibitor, rotenone, to increase mitochondrial ROS and then stimulated with nigericin. Although rotenone similarly increased mitochondrial ROS in WT, *Plscr3*$^{-/-}$ and *Crls1*$^{-/-}$ iBMDMs, rotenone modestly increased PI uptake in WT cells, but did not increase pyroptosis in *Plscr3*$^{-/-}$ or *Crls1*$^{-/-}$ cells (Figure S5L and S5M). Pyroptosis also was not enhanced in *Plscr3*$^{-/-}$ and *Crls1*$^{-/-}$ cells when other ETC complexes were inhibited (Figure S5N). Thus, mitochondrial ROS on its own cannot initiate pyroptosis in the absence of exposed cardiolipin.

ROS and pyroptosis increase OMM cardiolipin

Under basal conditions, cardiolipin is predominantly on the IMM but would need to be on the outer leaflet of the OMM to react with cytosolic GSDMD-NT to cause mitochondrial damage. Small amounts of OMM cardiolipin are reportedly present under basal conditions, but OMM cardiolipin increases during apoptosis[29,33]. We hypothesized that GSDMD-NT could initiate mitochondrial damage by binding to the few mitochondria that had exposed cardiolipin at baseline but that more mitochondria would quickly expose cardiolipin as mitochondrial damage ensued. To test this idea, we first examined whether mitochondria isolated from untreated cells have exposed cardiolipin by staining with anti-cardiolipin (Figure 6A and 6B). ~10% of isolated mitochondria stained for surface cardiolipin, and cardiolipin staining increased ~7-fold after Triton X-100 permeabilization, suggesting that the isolated mitochondria were intact and that at baseline some mitochondria expose cardiolipin, making it accessible to GSDMD-NT. When isolated mitochondria were treated with active GSDMD-NT, but not GSDMD-FL, cardiolipin externalization increased significantly within 45 min (Figure 6C). External cardiolipin MFI increased ~1.7-fold and 24% of mitochondria stained with anti-cardiolipin. Mitochondrial ROS induced in isolated mitochondria by mitochondrial

oxidants, antimycin A, rotenone or FCCP, also increased cardiolipin exposure (Figure 6D). Thus, GSDMD-NT and mitochondrial ROS, which is triggered by GSDMD-NT, increase cardiolipin exposure that could amplify GSDMD binding and mitochondrial damage. Because apoptosis has been reported to distribute cardiolipin to the plasma membrane[51], we next examined whether cardiolipin localization changed after adding nigericin by staining with the cardiolipin dye, Nonyl Acridine Orange (NAO) (Figure S6A). NAO-labeled cardiolipin colocalized with Mitotracker before and after triggering pyroptosis and did not stain the cell membrane, indicating that cardiolipin functions in mitochondria and does not integrate into the plasma membrane during pyroptosis.

Mitochondria release PNPT1 to cause global mRNA decay during pyroptosis

During apoptosis, MOMP releases PNPT1, an exoribonuclease in the IMS, to initiate global mRNA decay, which promotes apoptosis[34,52]. Because pyroptosis also triggers MOMP, PNPT1 would likely also be released to the cytosol and trigger mRNA decay during pyroptosis. To test this idea, PNPT1 localization was analyzed in LPS- and LPS+nigericin-treated iBMDMs by immunofluorescence microscopy and immunoblotting of fractionated cells (Figures 5F, 5G, 7A and 7B). PNPT1 localized to mitochondria in LPS-primed cells but moved to the cytosol after adding nigericin. As expected, PNPT1 release was blocked in *Plscr3*$^{-/-}$ and *Crls1*$^{-/-}$ iBMDMs (Figures 5F and 5G). By fluorescence in situ hybridization, probed for *18S* rRNA and poly(A) mRNA, the signal of mRNA became undetectable without a perceptible change in rRNA, in WT, but not *Plscr3*$^{-/-}$ and *Crls1*$^{-/-}$, iBMDMs treated with nigericin for 30 min (Figure 7C and 7D). Consistently, *Actb*, *Tuba* and *Sdha* housekeeping gene mRNAs sharply decreased within 30 min of adding nigericin or 60 min after *Salmonella* infection in WT, but not *Plscr3*$^{-/-}$ or *Crls1*$^{-/-}$, iBMDMs (Figure 7E). Moreover, ectopically expressed WT PLSCR3 and CRLS1, but not their inactive forms, in *Plscr3*$^{-/-}$ and *Crls1*$^{-/-}$ iBMDMs, respectively, restored pyroptotic mRNA decay induced by nigericin or *Salmonella* (Figure 7F and 7G). Thus, OMM cardiolipin is required for PNPT1-induced pyroptotic mRNA decay.

To investigate whether PNPT1-mediated mRNA decay contributes to pyroptosis, WT and *Pnpt1*$^{-/-}$ iBMDMs were treated with nigericin, LPS transfection or *Salmonella* (Figure 7H-K). *Pnpt1* deficiency significantly attenuated pyroptosis but did not affect nigericin-induced events upstream of PNPT1 release, including caspase-1 and GSDMD cleavage, GSDMD oligomerization and binding to mitochondria and the plasma membrane, or mitochondrial morphological change, ROS or mtDNA release (Figure S6B-I). To confirm that PNPT1 RNase activity is critical for promoting pyroptosis, WT or RNase-defective S484A PNPT1 were expressed in *Pnpt1*$^{-/-}$ iBMDMs[34] (Figure 7L). Ectopic WT, but not RNase-deficient, PNPT1, rescued nigericin-induced pyroptosis, indicating that PNPT1-mediated mRNA decay promotes pyroptosis.

Mitochondrial damage is required for GSDMA- and GSDME-mediated pyroptosis

Both GSDMA and GSDME are also reported to cause mitochondrial damage[22,53,54]. To evaluate the role of mitochondria in pyroptosis triggered by other GSDMs, GSDMA-NT or GSDME-NT were ectopically expressed in WT, *PLSCR3*$^{-/-}$, *CRLS1*$^{-/-}$ or *PNPT1*$^{-/-}$ HEK293T cells. LDH release and PI uptake by overexpressed GSDMA-NT or GSDME-NT were blunted in *PLSCR3*$^{-/-}$, *CRLS1*$^{-/-}$ or *PNPT1*$^{-/-}$ HEK293T cells (Figure S7A-F), indicating that mitochondrial damage enhances pyroptotic cell death induced by these other GSDMs.

To test whether OMM cardiolipin plays a role in other forms of programmed cell death, WT, *Plscr3*$^{-/-}$ and *Crls1*$^{-/-}$ iBMDMs were treated with etoposide, TNF-α+cycloheximide (CHX) or LPS+zVAD to induce intrinsic apoptosis, extrinsic apoptosis and necroptosis, respectively. Disrupting cardiolipin synthesis or OMM externalization did not affect apoptosis, but unexpectedly significantly

attenuated necroptosis (Figure S7G). Understanding the role of cardiolipin in necroptosis will require further study.

Discussion

Here we have shown that mitochondria are severely damaged during GSDMD-mediated pyroptosis in human and mouse macrophages by a BAX, BAX and mPTP-independent pathway. Mitochondrial damage depended on cardiolipin OMM exposure since all aspects of mitochondrial damage were virtually abrogated by cardiolipin synthase CRLS1 or scramblase PLSCR3 deficiency. GSDMD-NT permeabilized both mitochondrial membranes to cause profound morphological damage, disrupt electron transport, ATP generation and transmembrane potential, and induce ROS, mitophagy and release soluble mitochondrial proteins and mtDNA to the cytosol and culture medium. Moreover, ablation of either gene disrupted pyroptotic death, which could be rescued only with enzymatically active gene products. Mitochondrial ROS, which increases cardiolipin OMM exposure, enhanced pyroptosis, but was unlikely to be the only important factor since reducing mitochondrial ROS using the mitochondrial ROS scavenger MitoTEMPO or inducing cytosolic ROS by providing D-Ala to cells expressing a yeast D-amino oxidase had less of an effect on pyroptosis than genetic ablation of *Crls1* or *Plscr3*, and inducing ROS by mitochondrial toxins did not restore pyroptosis to *Plscr3* or *Crls1*-ablated cells.

Mitochondrial destruction occurs rapidly - virtually simultaneously with inflammasome activation and before cell membrane damage. We propose a simple 2-step model in which cleaved GSDMD quickly binds to OMM cardiolipin to assemble pores, permeabilizing the OMM, and then immediately binds to cardiolipin on the IMM, disrupting the IMM. In support of this model, GSDMD trafficked to mitochondria before it was detected on the cell membrane and both membranes were permeabilized when isolated mitochondria were incubated *in vitro* with caspase-11 and GSDMD. No other cytosolic proteins besides GSDMD-NT were needed to destroy mitochondria. Pyroptotic mitochondrial damage is more drastic than apoptotic damage, which doesn't directly damage the IMM, even though t-BID released more IMS proteins than GSDMD-NT *in vitro*.

Mitochondrial damage by GSDMD-NT may well be a "point-of-no-return" for pyroptosis, analogous to the role of MOMP in classical apoptosis. Under some circumstances, cells survive inflammasome activation and GSDMD-NT pore formation, even though they release inflammatory mediators, a process termed "hyperactivation"[2,11]. Mitochondrial damage in surviving hyperactivated cells may be more limited, leaving more functional mitochondria to supply cellular energy needs. In fact, noncanonical inflammasome activation in macrophages without cell death by oxidized phospholipids increased mitochondrial oxygen consumption and caused mitochondrial hypermetabolism[35]. Future studies should compare mitochondrial function in hyperactivated and pyroptotic cells. Differential mitochondrial damage could mean that the concentrations of activating stimuli, sensors or mediators of pyroptosis are reduced in hyperactivated cells or that unknown mechanisms for inhibiting pyroptotic mitochondrial damage exist in some cells.

The rapidity of mitochondrial damage, which begins as soon as caspase-1 activation and GSDMD cleavage are detected and before plasma membrane damage, may be linked to GSDMD-NT's high affinity for cardiolipin compared to plasma membrane phospholipids. Although we could not tell whether plasma membrane GSDMD-NT came from damaged mitochondria or the cytosol, the most plausible scenario is that damaged mitochondria and mitochondrial membrane-bound GSDMD-NT are removed and digested in mitophagosomes and that plasma membrane GSDMD-NT comes directly from cytosolic GSDMD-NT, which was still detected when we observed GSDMD membrane puncta. It has been suggested that NLRP3 inflammasomes assemble on mitochondria in a cardiolipin-dependent manner[55]. If that is the case, GSDMD cleavage could occur at the OMM

leading to rapid mitochondrial targeting of GSDMD-NT. Because mitochondrial damage and all its associated phenomena happen so quickly, we could not clearly identify the initial trigger. Although mitochondrial ROS was detected before other changes, it is unclear whether it was a trigger or just the first change detected. Some cardiolipin was present on the OMM basally and increased after treating mitochondria with active GSDMD or inducing ROS. This finding suggests that basal OMM cardiolipin initiates a pioneer round of GSDMD pore assembly, leading to ROS generation and more cardiolipin OMM exposure to amplify the pathway. HEK293T cells deficient in pyroptotic mitochondrial damage mediators have impaired GSDMA and GSMDE-mediated pyroptosis, confirming previous work that other GSDMs also damage mitochondria[22,53,54]. All the activated GSDMs likely trigger the same pyroptotic mitochondrial damage pathway as GSDMD. In fact, caspase-3-activated GSDME-NT permeabilizes mitochondrial membranes to augment neurite loss and/or cell death[22,54].

Pyroptotic mitochondrial damage is expected to amplify inflammation and immune responses to infection, tissue damage and cancer. Indeed, inhibiting mitochondrial damage attenuated anti-tumor immunity triggered by pyroptosis *in vivo*. Mitochondrial ROS amplifies NLRP3 activation[56] and triggers OMM transfer of cardiolipin[33]. Mitochondrial ROS may also contribute to pyroptosis by promoting GSDMD oligomerization and pore formation[28,42]. Two recent preprints suggest that GSDMD palmitoylation on human Cys191 or mouse Cys192 is required for activated GSDMD to form plasma membrane pores and cause cell death[57,58]. ROS increase palmitoylation by oxidizing unpaired Cys's and making them susceptible to palmitoylation. Mitochondrial ROS generated by GSDMD-mediated mitochondrial damage likely plays a critical role in promoting this post-translational modification and contributes to its important role in augmenting cell death. GSDMD-NT palmitoylation might also increase mitochondrial membrane binding.

Genetic ablation of *Plscr3* or *Crls1* in iBMDMs reduced SYTOX uptake and LDH release at 30 min by more than 2-fold, a sign of reduced plasma membrane permeabilization, but IL-1 release was completely blocked. IL-1β release requires both IL-1 processing and release through plasma membrane GSDMD pores, but genetic ablation of *Plscr3* or *Crls1* did not affect IL-1 processing, suggesting that mitochondrial damage plays a critical role in IL-1β release through GSDMD pores. We do not understand why IL-1β release is more strongly affected by suppressing mitochondrial damage than cell death. One possibility is that ROS more strongly promotes IL-1 secretion than pore formation, which merits further study. The strong dependence of IL-1β release on mitochondrial damage identifies an additional important way that mitochondrial damage amplifies *in vivo* inflammation.

OMM cardiolipin is a danger sign of mitochondrial damage[33]. Much like externalization of inner leaflet phosphatidyl serine to the cell membrane outer leaflet serves as an "eat-me-signal" for apoptotic cells, OMM cardiolipin serves as a mitophagy "eat-me-signal" for damaged mitochondria[29]. Additionally, externalized cardiolipin amplifies apoptosis as a docking site for caspase-8 and Bid to amplify Bid cleavage and promote MOMP pore formation by oligomerized BAX and BAK[59,60]. Cardiolipin oxidation on the IMS side of the IMM also promotes cytochrome c release[61]. The molecules released from the matrix and IMS during pyroptotic mitochondrial damage are also predicted to potently augment cell death and may also trigger other cell death pathways. Cytochrome c release should lead to apoptosome formation to activate caspase-3 to cleave Bid to cause BAK and BAX-mediated MOMP and cleave GSDME to amplify pyroptosis in GSDME-expressing cells. However, in our study, cell death was not reduced in BAX/BAK-deficient cells. Although activated caspase-3 can trigger apoptosis, apoptosis occurs more slowly than pyroptosis and is unlikely to occur if plasma membrane integrity has already been breached, since completing apoptosis requires a viable cell. Nonetheless activation of apoptosis could kill cells that

would otherwise be hyperactivated. As in apoptosis, release of mitochondrial PNPT1 during pyroptosis led to widespread mRNA degradation that contributed to cell death[34]. Although the mechanism for PNPT1 release is different in pyroptosis (GSDMD and cardiolipin-dependent vs BAX and BAK-dependent MOMP), once the enzyme gets into the cytosol, the same mechanism is operative - PNPT1 degradation of mRNA. mtDNA released into the cytosol during GSDMD-mediated mitochondrial damage is a potent danger signal that could be sensed to activate both cGAS and AIM2[18,37]. In support of this, noncanonical inflammasome activation secondarily activated the AIM2 inflammasome. Thus, GSDMD-mediated mitochondrial damage should increase cell commitment to death. Mitochondrial ROS, mtDNA and cardiolipin also function as damage-associated molecular patterns (DAMPs) to amplify inflammation. Oxidation of cardiolipin, mtDNA and other molecules by mitochondrial ROS could also promote other inflammatory and cell death pathways.

However, the amplifying effect of mitochondrial damage might only be physiologically important in some situations. For example, in response to nigericin, iBMDMs genetically ablated of *Crls1* and *Plscr3* did not show reduced ASC speck formation, caspase-1 cleavage or GSDMD-NT generation and oligomerization compared to WT iBMDMs or activate the AIM2 inflammasome. In contrast, noncanonical inflammasome activation by transfected LPS secondarily activated AIM2 specks. We interpret this difference to mean that secondary amplification by stronger inducers of pyroptosis may not occur or affect whether a cell dies but may become important for less potent inducers. Future studies should examine which secondary amplifying pathways are activated in different cell types and by different pyroptotic stimuli.

The GSDMD-NT-binding phospholipids in the plasma membrane are also present on the outer leaflets of endosomes, phagosomes, and lysosomes and cardiolipin is found on peroxisome membranes, suggesting that these other organelle membranes could be damaged during pyroptosis[62,63]. In macrophages undergoing pyroptosis, activated GSDMD was previously shown to damage both lysosomes and mitochondria before the plasma membrane[21]. The importance of lysosomes in regulating *Yersinia* infection-induced pyroptosis has been demonstrated recently - the lysosomal Rag-Ragulator complex serves as a platform to activate GSDMD in a pathway that involves TLR or death receptor signalling, RIPK1 and caspase-8[64]. It is worth investigating whether GSDM-NTs form pores on lysosomal and other organelle membranes and whether and how damage of other organelles contributes to pyroptosis.

A previous study used high-resolution imaging to show that mtDNA was released into the cytosol of living immortalized mouse embryonic fibroblasts treated with a BH3 mimetic drug to stimulate classical apoptotic BAK and BAX-dependent MOMP[65]. mtDNA release in this not-completely-physiological system was a rare event that occurred by herniation of the IMM through very large OMM “macropores” occasionally formed by BAX and BAK. The herniated IMM was presumed to burst but no mechanistic basis was defined. Our model of GSDMD-NT pores permeabilizing the IMM and causing mtDNA release describes a potential mechanism to disrupt the IMM. It is conceivable that mtDNA release observed in multiple settings might be mediated by GSDM disruption of mitochondrial membranes, especially since in addition to the inflammatory caspases, caspase-3 and caspase-8 can activate GSDME and GSDMD, respectively, and GSDMs can also be activated by other mislocalized or activated proteases in the cytosol[47,66-69].

Limitations of the Study

The experiments performed in this study implied that OMM and IMM were permeabilized by cardiolipin-dependent formation of GSDMD-NT pores in both membranes. Pore formation on both membranes was inferred from the rapid release of mitochondrial matrix and IMS contents and the fact that activated GSDMD-NT on its own could cause the same damage to isolated mitochondria

as in intact cells. Moreover, inhibiting GSDMD pore formation using disulfiram or *Gsdmd*$^{-/-}$ cells blocked mitochondrial permeabilization. However, our study did not visualize GSDMD-NT pores in these membranes. Although technically challenging, visualizing GSDM pores in mitochondrial membranes would provide direct evidence of GSDMD-NT pore formation in mitochondrial membranes.

Acknowledgments

We thank Derek Abbott, Case Western Reserve University, for providing mNeonGreen-GSDMD-expressing iBMDMs and the plasmid. Electron microscopy imaging was performed in the HMS Electron Microscopy Facility. Structured Illumination Microscopy imaging was performed in the HMS MicRoN microscopy core. Graphic abstract was created with BioRender.com. This work was supported by NIH R01CA240955 (J.L.), National Natural Science Foundation of China (32122034, 31972897), National Key R&D Program of China (2022YFC2304700, 2020YFA0509600), Key Research Program of the Chinese Academy of Sciences (ZDBS-LY-SM008), Shanghai Pilot Program for Basic Research-Chinese Academy of Sciences, Shanghai Branch (JCYJ-SHFY-2021-009), Strategic Priority Research Program of Chinese Academy of Sciences (XDB29030300), Shanghai Municipal Science and Technology Major Project (2019SHZDZX02, HS2021SHZX001), Innovative research team of universities in Shanghai (SHSMU-ZDCX20211002) (X.L.), National Natural Science Foundation of China (82125001), Research Program of Shanghai Pulmonary Hospital (fkcx1904) (P.Z.), the Cancer Research Institute Irvington Postdoctoral Fellowship (R.M.), NIH R01HL138475 (R.N.K.), T32HL144456 (F.G.L.), Ragon Early Independence Fellowship (C.L.E.), NIH R01HL152173 (T.M.) and Slovenian Research Agency (ARRS J3-1746 and P4-0176) (I.H.-B).

Author Contribution

R.M., C. Jiang, W.C., P.Z., X.L. and J.L. conceived the study. R.M., C. Jiang and W.C. designed and performed most experiments with assistance from H.Z., J.A., F.H., P.C., H.Z., C. Junqueira, D.A. and Y.P. and F.L. J.Z., C.L.E., I.H.-B., P.F., S.X., Z.Z., M.W-W., T.M., L.B-P., J.C.K., H.W. and R.N.K. provided technical support. R.M., C. Jiang, W.C., P.Z., X.L. and J.L. analyzed the data and wrote the manuscript. All authors discussed the results and commented on the manuscript. J.L. supervised the study.

Declaration of Interests J.L. and H.W. are cofounders and advisors of Ventus Therapeutics.

Figure Legends

Figure 1. Pyroptosis damages mitochondria.
(**A-B**) LPS-primed THP-1 were treated with nigericin for 1 h.
(**A**) Confocal fluorescence live cell images of LPS+nigericin-treated THP1 stained with MitoTracker Deep Red (MTDR), MitoTracker green (MTG) and PI (left) or TMRM, MTG and SYTOX Deep Red (SYTOX DR) (right). White arrows indicate pyroptotic cells. Scale bar: 5 μm.
(**B**) Relative mean fluorescence intensity (MFI) of MTDR and TMRM in PI or SYTOX negative and positive cells, normalized to MTG.
(**C-D**) LPS-primed THP-1 were treated with nigericin for indicated times. Transmission electron microscopy images of LPS+nigericin-treated THP1 at indicated times (**C**). Lower panels show higher magnification of the boxed area in upper panels. Black arrows indicate normal mitochondria; yellow arrows, mitochondria with loss of cristae or membrane damage; red arrow, damaged mitochondria within an autophagosome. Scale bars: 500 nm. Mitochondrial (mito) mean length and number, percentage of damaged mitochondria, and mitophagosome number were quantified (**D**).
(**E-G**) THP-1 were LPS+nigericin-treated for indicated times. Immunoblots probed for indicated proteins in cytosolic and mitochondrial fractions and culture supernatants (**E**) and densitometry of 3 independent experiments (**F**). (**G**) Cytosolic mtDNA by qPCR, normalized to time 0.
Data are mean ± s.d. of at least 50 cells (**B**), 8 cells or 50 mitochondria (mean length) or at least 100 mitochondria (percentage of damaged mitochondria) (**D**), or biological triplicates (**F, G**), and are representative of 3 independent experiments, analyzed by two-tailed Student's *t*-test (**B, D**) or one-way ANOVA using the Holm-Sidak method for multiple comparisons (**G**). **P<0.01; ***P<0.001. Please also see Figure S1.

Figure 2. Mitochondrial damage occurs before plasma membrane damage and enhances pyroptosis.
(**A**) Kinetic analysis of DCF and TMRM intensity and SYTOX green uptake in LPS- or LPS+nigericin-treated THP-1 by plate reader. * indicate first time the variable significantly changed.
(**B**) Flow cytometry histograms (top) and quantification of multiple samples (bottom) of LPS+nigericin-treated THP1 stained with MitoSOX, DiIC1(5) or SYTOX Green. P: positive control (Antimycin A for MitoSOX, CCCP for DiIC1(5), and Triton X-100 for SYTOX Green); UNT: untreated.
(**C-E**) iBMDMs were untreated (UNT) or treated with ethidium bromide (EB) for 5 days. (**C**) Confocal fluorescence images (left) and MitoTracker MFI quantification in individual cells (right). Cell death by LDH release (**D**) or CellTiter-Glo assay (**E**) 1 h after adding LPS+nigericin (**D**) or LPS transfection (trans) (**E**).
(**F-I**) iBMDMs, pre-treated with MitoTEMPO for 30 min, were treated with nigericin (**F, G**), LPS transfection (**H**), or poly(dA:dT) (**I**). Cell death was measured by SYTOX green uptake (**F**) or CellTiter-Glo assay (**G-I**).
(**J-L**) iBMDMs stably expressing HyPer7-DAAO-nuclear export signal (NES) (**J, K**) or HyPer7-DAAO-nuclear localization sequence (NLS) (**L**) were pre-incubated with D- or L-alanine for 4 h. (**J**) Confocal fluorescence images (left) and the quantification of their ratio in multiple experiments (right). (**K, L**) LPS+nigericin-induced cell death in cells expressing Hyper7-DAAO-NES (**K**) or Hyper7-DAAO-NLS (**L**) assessed by SYTOX green uptake.
Data are mean ± s.d. of 100 cells (**C**), 30 cells (**J**), or biological triplicates, and are representative of 3 independent experiments, analyzed by multiple *t*-tests (**A**), two-tailed Student's *t*-test (**C, J**) or one-way ANOVA using the Holm-Sidak method for multiple comparisons (**B, D-I, K, L**). *P<0.05; **P<0.01; ***P<0.001. Please also see Figure S1.

Figure 3. GSDMD-NT translocates to and damages mitochondria before the plasma membrane.

(**A-B**) Mitochondrial damage and cell death assessed by live cell imaging of iBMDMs stably expressing DOX-inducible GSDMD-NT(I105N)-BFP and co-stained with MitoTracker Deep Red and PI (**left**), TMRM and SYTOX Deep Red (SYTOX DR) (**middle**) or MitoSOX Red and PI (**right**), imaged beginning 6 h after adding DOX. Time 0 indicates first detection of PI or SYTOX in the cell (blue dashed lines). Scale bar: 2 μm. Time lapse images (**A**) and quantification of relative fluorescence dye intensity in individual cells (**B**).
(**C-E**) HEK293T transiently transfected to express Flag-GSDMD-FL or Flag-GSDMD-NT and analyzed 18 h later. (**C**) Confocal fluorescence images stained for COX IV, Flag and DAPI (left). XZ and YZ projections are shown. Scale bar: 5 μm. Quantification of Pearson's correlation of COX IV and Flag (right). (**D**) Structured Illumination Microscopy (SIM) images stained for COX IV and Flag. Higher magnification images and 3D rendering of the boxed area are shown. Scale bar: 5 μm or as indicated. (**E**) Transmission electron microscopy images stained with Flag-immunogold (left). Lower panels show higher magnification of the boxed area in upper panels; yellow dashed lines outline mitochondria. Scale bar: 500 nm. Quantification of gold particles in mitochondria (mito) versus cytosol (right).
Data are mean ± s.d. of 3 cells (**B**), at least 30 cells (**C**) or at least 30 mitochondria (**E**), and are representative of 3 independent experiments, analyzed by two-tailed Student's *t*-test. ***P<0.001. Please also see Figures S2 and S3.

Figure 4. GSDMD-NT permeabilizes and damages isolated mitochondria.
Mitochondria isolated from HCT116 (**A-E**) or iBMDMs (**F-G**) treated with GSDMD and/or caspase-11 or t-Bid in the presence or absence of z-VAD-FMK or disulfiram (DSF) for 45 min or indicated times.
(**A, B, F**) Immunoblots of post-treatment supernatant or mitochondria (**A, F**) and densitometry of multiple experiments (**B**).
(**C, G**) mtDNA in supernatants by qPCR, normalized to untreated mitochondria.
(**D, E**) Flow cytometry histograms of MitoSOX Red (**D**) or DiIC1(5) (**E**) stained mitochondria (left) and quantification of MFI of treated mitochondria, relative to MFI of untreated mitochondria (right). CCCP and antimycin A were positive controls.
Data are mean ± s.d. of biological triplicates, and are representative of 3 independent experiments, analyzed by one-way ANOVA using the Holm-Sidak method for multiple comparisons. **P<0.01; ***P<0.001.

Figure 5. OMM cardiolipin is required for GSDMD-mediated mitochondrial damage, pyroptosis, and anti-tumor immune response.
(**A**) Schematic of cardiolipin synthesis and translocation.
(**B**) Confocal live cell imaging of LPS- or LPS+nigericin-treated WT, *Plscr3*$^{-/-}$ or *Crls1*$^{-/-}$ iBMDMs expressing mNG-GSDMD, stained for MitoTracker Deep Red 30 min after adding nigericin. White arrows indicate mitochondrial recruitment of GSDMD. Pearson's correlation of MitoTracker and mNG-GSDMD (right).
(**C-M**) LPS-primed WT, *Crls1*$^{-/-}$ or *Plscr3*$^{-/-}$ iBMDMs were treated with nigericin. (**C**) Confocal live cell images stained for MitoTracker Deep Red (MTDR), MitoTracker green (MTG) and PI (left) or TMRM, MTG and SYTOX Deep Red (SYTOX DR) (middle) 1 h after nigericin treatment (Scale bar: 5 μm) and quantification of relative mean fluorescence intensity (MFI) of MTDR and TMRM (right).
(**D, E**) Transmission electron microscopy images 1 h after adding nigericin (**D**) and quantification of mitochondrial (mito) number, mean length and damaged mitochondria (**E**). Lower panels show magnification of the area marked in upper panels. Black arrows, normal mitochondria; yellow arrows, mitochondria with loss of cristae or membrane damage. Scale bars: 500 nm. (**F, G**) Immunoblots of whole cell lysates (WCL), cytosolic (cyto) and mitochondrial (mito) fractions of LPS-primed iBMDMs 30 min after no treatment or nigericin. (**H, I**) Cytosolic mtDNA by qPCR

normalized to untreated WT cells. (**J-M**) Cell death by PI uptake (**J**, **L**) or LDH release after 30 min (**K**, **M**).
(**N-P**) Comparison of growth of subcutaneous WT J774 tumors injected after mixing with LPS+nigericin- or mitomycin C (MMC)-pretreated, WT or *Plscr3*$^{-/-}$ J774. (**N**) Immunoblot of control (CTL) WT or *Plscr3*$^{-/-}$ J774 lysates probed for PLSCR3 and β-actin. (**O**) SYTOX green uptake after *in vitro* treatment with LPS or LPS+nigericin. (**P**) WT J774 tumor volume after mixing with LPS+nigericin (left) or MMC (right) pretreated CTL or *Plscr3*$^{-/-}$ J774. Data are mean ± SEM of 5 mice and are representative of 2 independent experiments. The area under the curve was compared by two-tailed Student's *t*-test.
Data are mean ± s.d. of at least 30 cells (**B, C**), 8 cells or 50 mitochondria (mean length) or at least 100 mitochondria (percent damaged mitochondria) (**E**), or biological triplicates (**H-M, O**), and are representative of 3 independent experiments unless otherwise indicated, analyzed by one-way ANOVA using the Holm-Sidak method for multiple comparisons. *P<0.05; **P<0.01; ***P<0.001. Please also see Figures S4 and S5.

Figure 6. OMM cardiolipin is weakly exposed under basal conditions but increases in response to mitochondrial oxidants or activated GSDMD.
HEK293T isolated mitochondria were treated with Triton (**B**), GSDMD engineered with a linker 3C proteinase cleavage site and/or 3C proteinase (**C**), or mitochondrial poisons [Antimycin A (AA), Rotenone (Rot) or FCCP] (**D**) for 45 min and stained with MitoTracker Green and anti-cardiolipin.
(**A**) Flow cytometry gating strategy for isolated mitochondria.
(**B-D**) Flow cytometry histograms of anti-cardiolipin stained mitochondria (left), quantification of cardiolipin MFI relative to untreated (UNT) mitochondria (middle), and percentage of cardiolipin+ mitochondria (right). UNS: unstained, ISO: isotype staining control without treatment; UNT: untreated control stained for cardiolipin.
Data are mean ± s.d. of biological triplicates, and are representative of 3 independent experiments, analyzed by one-way ANOVA using the Holm-Sidak method for multiple comparisons. *P<0.05; **P<0.01; ***P<0.001.

Figure 7. Pyroptosis causes cardiolipin-dependent PNPT1 release and mRNA decay.
(**A, B**) (**A**) Confocal fluorescence images of iBMDMs, primed with LPS and then treated or not with nigericin for 30 min, and stained for MitoTracker Deep Red, PNPT1 and DAPI. Scale bar: 5 μm.
(**B**) Pearson's correlation of MitoTracker and PNPT1.
(**C, D**) Poly(A) mRNA and *18S* rRNA visualized by FISH in indicated LPS-primed iBMDMs treated or not with nigericin for 30 min. Confocal images (**C**) and quantification of the fluorescence intensity of poly(A) versus *18S* (**D**). Scale bar: 20 μm.
(**E-G**) WT, *Crls1*$^{-/-}$ or *Plscr3*$^{-/-}$ iBMDMs, rescued to express WT or mutant PLSCR3 (**F**) or CRLS1 (**G**) or neither (**E**) were treated with LPS or LPS+nigericin for 30 min or infected with *Salmonella* for 1 h. Housekeeping gene mRNAs relative to *7SL* and normalized to the ratio in untreated WT cells.
(**H-L**) Effect of *Pnpt1* genetic ablation on pyroptosis. (**H**) Immunoblot of iBMDM cell lysates of control (CTL) WT or *Pnpt1*$^{-/-}$ clones. Pyroptosis in WT or *Pnpt1*-deficient after treatment with LPS or LPS+nigericin by SYTOX Green (**I**), LPS electroporation by CellTiter-Glo (**J**), or *Salmonella* infection by LDH release (**K**). (**L**) *Pnpt1*$^{-/-}$ iBMDMs, rescued with empty vector (EV), WT or RNase-defective PNPT1, were analyzed for PI uptake after treatment with LPS or LPS+nigericin. PNPT1 expression by immunoblot (right).
Data are mean ± SEM of at least 50 cells (**B**), 5 images (**D**), or biological triplicates, and are representative of 3 independent experiments, analyzed by two-tailed Student's *t*-test (**B**), one-way ANOVA using the Holm-Sidak method (**D, I- L**), or two-way ANOVA using the Tukey method (**E-G**) for multiple comparisons. ***P<0.001. Please also see Figures S6 and S7.

STAR Methods

Resource availability

Lead contact

Requests for resources, reagents and further information should be directed to the lead contact, Judy Lieberman (judy.lieberman@childrens.harvard.edu).

Materials availability

All plasmids and cell lines used in this study are available from Addgene or the lead contact.

Experimental model and subject details

Cell culture

Mouse iBMDMs, HCT116 and HEK293T were cultured in DMEM (Invitrogen). THP-1 were cultured in RPMI-1640 (Corning). Media were supplemented with 10% heat-inactivated fetal bovine serum, 100 U/mL penicillin G, 100 µg/mL streptomycin sulfate, 6 mM HEPES, 1.6 mM L-glutamine and 50 µM 2-mercaptoethanol. Cells were verified to be free of mycoplasma contamination. Inducible GSDMD-NT-BFP expressing iBMDMs were generated as previously described[28] and cultured in complete DMEM media supplemented with 10 µg/ml puromycin and 1.5 mg/ml G-418.

Bacteria

Glycerol stocks of *Salmonella typhimurium* strain were streaked on Luria-Bertani (LB) agar plates. Single colonies were picked and cultured in LB liquid medium overnight. On the day of infection, bacteria were diluted 1:50 into LB medium and grown to logarithmic phase for 4 h, before adding to cells in a multiplicity of infection (MOI) of 10. Infection was facilitated by centrifugation at 400 g for 5 min and incubation at 37°C for ~30 min. Extracellular bacteria were killed by adding 50 µg/mL gentamicin. Cell death induced by *Salmonella typhimurium* infection was assessed 1 h post infection.

Mice:

6-8 wk old female BALB/c mice were purchased from Jackson Laboratories and housed in the Harvard Medical School Animal Facility. All procedures were conducted in compliance with all the relevant ethical regulations and were approved by the Animal Care and Use Committees of Boston Children's Hospital and Harvard Medical School.

Method details

Cell treatment

THP-1 cells were differentiated by treatment with 50 ng/mL phorbol 12-myristate 13-acetate (PMA) for 36-48 h. To induce NLRP3-dependent pyroptosis, differentiated THP-1 cells and iBMDMs were primed with 1 µg/mL LPS for 4 h, and then stimulated with 20 µM nigericin or 5 mM ATP. To trigger non-canonical and AIM2 inflammasome-mediated pyroptosis, iBMDMs were transfected with 1 µg LPS or poly (dA:dT), respectively, using the Amaxa Mouse Macrophage Nucleofection Kit (Lonza) according to the manufacturer's instructions. Transient transfection of HEK293T was performed by calcium phosphate precipitation or using the X-tremeGENE™ HP DNA Transfection Reagent (Roche) according to the manufacturer's instructions. To inhibit the NLRP3 inflammasome, iBMDMs were pre-treated with 500 nM MCC950 for 30 min before stimulation with LPS or poly (dA:dT) transfection. mPTP was inhibited by pre-incubating iBMDMs with 25 µM BKA (ANT), 1 µM CsA (cyclophilin D), 5 µM VBIT-4 (VDAC) or 1 µM NEM (PiC) for 30 min before stimulation with nigericin. To inhibit electron transport chain (ETC) complexes, iBMDMs were pretreated with 5 µM rotenone (complex I) for 1 h, 1 µM Piericidin A (complex I) for 40 min, 10 µM TTFA (complex II) for 6 h, 1 µM antimycin A (complex III) for 6 h, or 1 µM oligomycin (complex V) for 6 h before adding nigericin.

Live cell confocal imaging
$5x10^5$ THP-1 or iBMDMs were seeded in 35 mm imaging dishes (MatTek, p35g-1.5-10-c) 18-24 h before treatment. For inducible GSDMD-NT-BFP iBMDMs, 2 μg/ml doxycycline was added to induce protein expression for 4-6 h before imaging. mNG-GSDMD-expressing iBMDMs were primed with 1 μg/ml LPS for 3 h and then treated with 20 μM nigericin for 30-45 min. Cells were stained with 200 nM MitoTracker Deep Red (MTDR), 200 nM MitoTracker green, 100 nM TMRM, 200 nM MitoSOX Red or 200 nM NAO for 30 min at 37°C. 200 nM SYTOX Green, 200 nM SYTOX Deep Red, or 500 nM PI was added to cell medium immediately before imaging. Cells were imaged in a heated chamber (37°C, 5% CO_2) on a Zeiss 880 laser scanning confocal microscope with 63x oil immersion objective and analyzed using Zeiss Zen software. Fluorescence intensity and Pearson's correlation coefficient were analyzed using Zeiss Zen software. The enrichment of mNG-GSDMD on the plasma membrane was quantified by measuring the mean fluorescence intensity of mNG-GSDMD in three randomly selected regions on the plasma membrane versus in the cytosol.

Transmission electron microscopy
LPS and nigericin treated THP-1 or iBMDMs were fixed (2.5% paraformaldehyde, 2.5% glutaraldehyde, 0.05% picric acid in 0.2 M cacodylate buffer) for at least 2 h, washed in 0.1 M cacodylate buffer, post-fixed (1% osmium tetroxide, 1.5% potassium ferrocyanide) for 1 h, washed twice in water, once in maleate buffer (MB) and incubated in 1% uranyl acetate in MB for 1 h, followed by two washes in water and subsequent dehydration in alcohol (10 min each; 50%, 70%, 90%, 2x 100%). The samples were then placed in propylene oxide for 1 h and infiltrated in a 1:1 mixture of propylene oxide and TAAB Epon (TAAB Laboratories Equipment Ltd., T004). The following day, samples were embedded in TAAB Epon and polymerized at 60°C for 48 h. 60 mm sections were cut on a Reichert Ultracut-S microtome and placed onto copper grids stained with lead citrate and imaged using a TecnaiG² Spirit BioTWIN electron microscope with an AMT 2k CCD camera at 3,000x and 10,000x magnification. Mitochondrial and autophagosomal numbers were counted manually and mitochondrial length was measured by ImageJ software. Damaged mitochondria were identified by loss of cristae and/or broken mitochondrial outer and/or inner membrane.

Cell fractionation
Differentiated and primed THP-1 or primed iBMDMs were detached using 0.25% Trypsin-EDTA (ThermoFisher, 25200056), washed twice with PBS and resuspended in PBS. Cells were then treated with 20 μM nigericin at 37°C for indicated times. Culture supernatants and cell pellets were collected. To fractionate cells, cell pellets were resuspended and incubated in isotonic buffer A (10 mM Tris-HCl pH 7.5, 10 mM KCl, 250 mM sucrose, 1.5 mM $MgCl_2$) on ice for 15 min and then homogenized using a glass homogenizer for 30 strokes. Nuclear fractions were removed by centrifugation (1,000 g, 10 min, 4°C) and mitochondrial fractions were pelleted by centrifugation of the post-nuclear supernatant (7,000 g, 10 min, 4°C) and the supernatants were collected as the cytosol fraction.

Immunoblot
Whole cell pellets, mitochondrial fraction and post-treatment mitochondrial pellets of isolated mitochondria were lysed with lysis buffer (50 mM Tris-HCl pH7.5, 150 mM NaCl, 1 mM EDTA, 1% Triton X-100) supplemented with a complete protease inhibitor cocktail (Roche) at 4°C for 20 min. Supernatants were collected after centrifugation at 18,500 g for 20 min at 4°C. For detecting GSDMD-NT oligomerization, cells were lysed with lysis buffer containing 30 mM N-ethylmaleimide and the cell lysates were prepared with SDS loading buffer without β-mercaptoethanol. Samples were subjected to electrophoresis through SDS-polyacrylamide electrophoresis gels. The

separated proteins were then transferred to a polyvinylidene fluoride membrane (Millipore). Immunoblots were probed with the indicated antibodies and visualized by SuperSignal West Femto Maximum Sensitivity Substrate (Thermo Scientific) and the ChemiDoc MP Imaging System (BioRad). Densitometry was measured using ImageJ and quantified relative to the strongest band.

mtDNA release assay

DNA was extracted from fractionated cytosolic fractions or post-treatment supernatants of isolated mitochondria using the DNeasy Blood & Tissue Kit (Qiagen) according to the manufacturer's instructions. mtDNA amounts were quantified by qRT-PCR using SsoFast EvaGreen Supermix (BioRad, 172-5204) and a BioRad iCycler. Measurements were normalized to *GAPDH* or *18S* rRNA amounts.

Seahorse metabolic analysis

$1x10^5$ cells/well of differentiated THP-1 were seeded on a Seahorse 96-well plate in DMEM supplemented with 10% FBS and primed or not with LPS for 4 h. After 24 h, cells were washed twice and incubated in the Seahorse Assay Medium supplemented with 25 mM glucose and 2 mM glutamine at 37°C for 45 min. Indicated concentrations of nigericin were injected at time 0. The OCR and ECAR were measured under basal conditions and after injection of 1.5 µM oligomycin, 1.5 µM FCCP and 0.5 µM rotenone plus 0.5 µM antimycin A using a Seahorse XFe96 Extracellular Flux Analyzer (Agilent).

Microplate reader assays

$1x10^5$ cells/well of differentiated THP-1 or iBMDMs were seeded on 96-well plate and primed as described above. Mitochondrial transmembrane potential and ROS were assessed by TMRM staining (Invitrogen, I34361) and the DCFDA Cellular ROS Assay Kit (Abcam, ab113861), respectively, according to the manufacturer's instructions. Briefly, prior to the end of priming, cells were pre-stained with 25 µM DCFDA for 45 min or 200 nM TMRM for 30 min. 5 µM FCCP and 50 µM Tert-butyl hydrogen peroxide (TBHP) were used as positive controls for membrane potential and ROS assays, respectively. To measure plasma membrane permeabilization, the cell culture medium was replaced with medium containing 1 µM SYTOX Green or buffer B (120 mM NaCl, 4 mM KCl, 1.5 mM $CaCl_2$, 1 mM $MgCl_2$, 25 mM HEPES, 5 mM glucose, and 0.1% BSA, pH 7.4) containing 2 µg/ml PI. Readings were normalized to control wells incubated with 0.05% Triton X-100. Kinetic readings (2.5 min intervals, 37°C) were recorded at the recommended excitation/emission wavelengths using a Synergy H4 Hybrid Multi-Mode Microplate Reader (BioTek).

Cell death and viability were determined 1.5 h (unless otherwise indicated) after nigericin or ATP treatment, or 2.5 h after LPS- or poly(dA:dT)-transfection by measuring LDH release using the CytoTox 96 Non-Radioactive Cytotoxicity Assay (Promega, G1780) or cellular ATP using the CellTiter-Glo Luminescent Cell Viability Assay (Promega, G7570), respectively. Luminescence and absorbance were measured on a Synergy H4 Hybrid Multi-Mode microplate Reader.

Flow cytometry

Differentiated THP-1 were detached using 0.25% Trypsin-EDTA, collected in PBS and stained with 500 nM MitoSox Red or 50 nM DiIC1(5) for 30 min at 37°C, followed by washing in PBS. Cells were then treated with 20 µM nigericin for indicated times and analyzed on a FACSCanto II flow cytometer using FlowJo software. 50 µM Antimycin A and 50 µM CCCP were used as positive controls for ROS and transmembrane potential, respectively. To assess plasma membrane permeabilization, 200 nM SYTOX Green was added to the cell suspension prior to treatment with nigericin. 0.05% Triton X-100 was used as a positive control.

Generation of mitochondria-deficient ρ° iBMDMs
To obtain mitochondria-deficient ρ° cells, iBMDMs were treated with 100 ng/mL ethidium bromide (EB) for 5 days.

MitoTEMPO treatment
For nigericin-induced pyroptosis, iBMDMs were primed with 1 μg/mL LPS for 4 h and 30 min before the end of priming, cells were pre-incubated with 500 μM MitoTEMPO for 30 min before adding 20 μM nigericin. For LPS and poly(dA:dT) transfection, iBMDMs were dissociated from the culture dish by trypsinization and collected in PBS. Cell suspensions were incubated with 500 μM MitoTEMPO for 30 min and washed once with PBS. Cells were then nucleofected as described above.

Plasmids
The HyPer7-DAAO-NES and HyPer7-DAAO-NLS fragments[40] were inserted into the pLenti-CMV-BLAST lentiviral vector. cDNAs for *Crls1* and *Plscr3* were amplified by polymerase chain reaction (PCR) from the mouse cDNA library and cloned into a modified pHAGE lentiviral vector with a 3xFlag tag at the N-terminus. All point mutations were generated by overlap PCR cloning. All plasmids were verified by sequencing.

Stable cell lines
To generate lentiviruses, a lentiviral vector containing the gene of interest was transfected into HEK293T together with psPAX2 and pCMV-VSV-G at a 10:9:1 ratio. Supernatants collected 2 days later were used to transduce iBMDMs for 2-3 days. 10 μg/ml blasticidin was added to select for stable expression.

Chemogenetic activation of DAAO and production of ROS
iBMDMs stably expressing HyPer7-DAAO were incubated with 10 mM D- or L-alanine together with 10 μM flavin adenine dinucleotide (FAD, Sigma) and 1 μg/mL LPS for 4 h before treatment with 20 μM nigericin. ROS was assessed by the ratio of oxidized (excited at 480 nm)/reduced (excited at 420 nm) HyPer7, acquired at an emission wavelength of 530 nm using live cell confocal imaging.

Immunostaining and confocal microscopy
iBMDMs (0.4 x 10^6 cells/well) or HEK293T (0.3 x 10^6 cells/well) were seeded and grown on coverslips in 12 well plates. 500 nM Mitotracker Orange/Red was pre-incubated for 15 min at 37°C before fixation with 4% paraformaldehyde (PFA) for 15 min. Cells were permeabilized with 0.1% Triton X-100 for 10 min at room temperature and blocked with 5% BSA in PBS for 1 h. Cells were then incubated with indicated primary antibodies overnight at 4°C, followed by incubation with the corresponding fluorescent-conjugated secondary antibodies for 1 h (Invitrogen). Nuclei were counterstained with 4,6-diamidino-2-phenylindole (DAPI; Invitrogen). Slides were mounted using Fluorescence Mounting Medium (ThermoFisher). Images were captured using an Olympus Fluoview FV1000 Confocal System with 60x oil immersion objective or a Zeiss 880 Laser Scanning Confocal Microscope with 63x oil immersion objective and analyzed using Olympus Fluoview software or Zeiss Zen software. MitoTracker fluorescence intensity was measured using ImageJ software (Figure 2C). Pearson's correlation coefficient was analyzed using Zeiss Zen software.

Structured Illumination Microscopy (SIM)
Samples were imaged on a Nikon Ti-E inverted widefield microscope equipped with a fully motorized stage and perfect focus system. Images were acquired using a 1.45 NA Plan Apo ×100 Ph3 DM objective lens with Cargille Type 37 immersion oil. Fluorescence was excited using a Lumencore SpectraX LED light engine and filtered using ET-GFP (Chroma, 49002) and ET-

mCherry (Chroma, 49008) filter sets. Images were captured on an Andor Zyla 4.2 Plus sCMOS camera (65 nm pixel size) using Nikon Elements (v5.10) acquisition software. Z-stack images were drift corrected using a customized StackReg plugin in Fiji. Subsequently, fluorescence images were deconvolved using the classical maximum likelihood estimation algorithm in Huygens Essential v19.10 (SVI), employing an experimentally derived point spread function (PSF) from 100 nm TetraSpeck beads (Thermo Fisher Scientific). Image reconstruction and 3D rendering was conducted using Arivis Vision4D software.

Immunogold-electron microscopy

Cells were washed once with PBS and gently removed from the culture dish by pipetting up and down. ~1 ml of the cell suspension was layered on a 200 µl cushion of 4% PFA/0.1% Glutaraldehyde (in 0.1 M Sodium Phosphate buffer, pH 7.4) in an Eppendorf tube and pelleted for 3 min at 3000 rpm. The supernatant was discarded and fresh 4% PFA/0.1% glutaraldehyde was gently layered on the pellet without resuspension. After 1 h fixation at room temperature, fixative was replaced with PBS and the cell pellet was infiltrated with 2.3 M sucrose in PBS (containing 0.2 M glycine to quench free aldehyde groups) for 15 min. Samples were then frozen in liquid nitrogen and sectioned at -120°C. Sections were transferred to formvar-carbon coated copper grids and the grids were floated on PBS at 4°C for immunogold labeling. Gold labeling was carried out at room temperature on a piece of parafilm. Grids were blocked by floating on drops of 1% BSA for 10 min and then incubated with drops of 5 µl primary antibody (diluted in 1% BSA in PBS) for 30 min at room temperature. Grids were washed with PBS for 15 min, incubated with Protein-A gold (diluted in 1% BSA) for 20 min and washed in PBS for 15 min. Contrasting/embedding of the labeled grids was carried out on ice in 0.3% uranyl acetate in 2% methyl cellulose for 10 min. Grids were picked up with metal loops (diameter slightly larger than the grid) and the excess liquid was removed by streaking on a filter paper, leaving a thin coat of methyl cellulose (bluish interference color when dry). The grids were examined in a JEOL 1200EX Trans electron microscope and images were recorded with an AMT 2k CCD camera. The enrichment of immunogold particles on mitochondria was quantified manually by counting the number of particles in mitochondria and in three randomly selected surrounding cytosolic regions of the same area as the mitochondrion. The enrichment on mitochondria was quantified as the ratio of particle number in each mitochondrion versus the average particle number in three cytosolic regions.

Isolation and treatment of mitochondria

HCT116 were washed in PBS and collected with gentle scraping. Mitochondria, obtained as described in the cell fractionation protocol, were resuspended in twice the volume of Buffer A and treated with 5 µM recombinant human GSDMD and/or 5 µM caspase-11, purified as previously described[70], or 7.5 µg/mL recombinant mouse t-BID (Prospec; pro-644) in the presence or absence of 5 µM z-VAD-FMK (BD Pharmingen, 550377) or 20 µM DSF and incubated for indicated times at 37°C with shaking. Treated mitochondria were pelleted (7,000 g, 4°C, 20 min), and the post-treatment supernatants and mitochondrial pellets were collected.

Membrane surface cardiolipin staining of isolated mitochondria

Isolated mitochondria from HEK293 T were resuspended in 5x volume of FACS buffer (PBS+5% BSA) and treated with 0.05% Triton X-100, 10 µM rotenone, 50 µM antimycin A, 20 µM FCCP, or 5 µM GSDMD and/or 0.5 µM 3C protease[8] for 45 min on a heated shaker at 37 °C, 350 rpm. 500 nM MitoTracker green was added 20 min before the end of treatment. Treated mitochondria were incubated with anti-cardiolipin serum (USBiological) at 1:1000 on ice for 15 min, followed by incubation with APC-conjugated anti-human secondary antibodies for 15 min (Jackson ImmunoResearch). The mitochondria were then analyzed on a FACSCanto II flow cytometer using FlowJo software. Mitochondrial events were gated using MitoTracker green. Cardiolipin exposure

was measured by cardiolipin MFI and calculated as (X-Iso)/(Triton-Iso) x100 and normalized to untreated control.

Generation of genetically ablated cells by CRISPR-Cas9
Lentiviruses carrying Cas9- and sgRNA-expressing lentiCRISPR v2 were produced in HEK293T, as previously described[64,71]. Cells were infected with the lentivirus and then selected with 5 μg/ml puromycin (iBMDMs, 293T) or 2 μg/ml blasticidin (J774). Surviving cells were cloned and gene ablation in clones was verified by sequencing genomic DNA and immunoblotting. sgRNA sequences for the targeted genes were as follows: *Crls1* (5'-ATA CCG AAC TCT GCC AAC AC-3'/5'-ATG GAT TTA TTG CTC GAA AC-3'), *Plscr3* (5'-ACT GGA GCT TGT CCC GGT CC-3'/5'-TCC GCT AGG CGG ATT CGA AA-3'), control sgRNA (5'-GCC TGC CCT AAA CCC CGG AA-3' or 5'-GCG AGG TAT TCG GCT CCG CG-3'), *Pnpt1* (5'-GTG TCG TTA ACC CAA CA-3'/5'-GCC TTC CCA ATT CAT GCC GT-3'), *BAX* (5'-AGT AGA AAA GGG CGA CAA CC-3', Addgene 129580), *BAK* (5'-GCC ATG CTG GTA GAC GTG TA -3', Addgene 129579), *PLSCR3* (5'- ACA GGC TAC TTG CCC CCC AA-3'/5'-CCA GGA TGT AGC GCC GGC TC-3'), *CRLS1* (5'-ATG TTG TCA ATG ACG AGA AT-3'/5'-ATG GAT TTA TTG CTC GAA AC-3') and *PNPT1* (5'- GAA GGA AAG GAC CAT CGC TC-3'/5'-GTG AGT GCC CGA TCC CGC CG-3').

MitoSOX staining
Mitochondrial ROS was measured using MitoSox Red (Invitrogen, M36008) according to the manufacturer's instructions. Briefly, LPS-primed iBMDMs were incubated with 5 μM MitoSOX for 10 min at 37°C and then treated with nigericin (40 μM). Fluorescence was read by plate reader using excitation and emission wavelengths of 510 and 580 nm, respectively.

ELISA
iBMDMs were treated as indicated and cell supernatants were collected 30 min after nigericin stimulation. IL-1β release was measured using the Mouse IL-1 beta/IL-1F2 Quantikine ELISA Kit (R&D Systems, MLB00C) according to the manufacturer's instructions.

Mouse studies
Control sgRNA (CTL) and *Plscr3*$^{-/-}$ J774 were primed with 1 μg/ml LPS for 3 h and then treated with 20 μM nigericin for 2 h or were treated with 60 μM mitomycin C (MMC) for 20 h to induce ~60-70% cell death. Both live and dead cells were collected and washed once with PBS. 1x10^5 MMC or LPS+nigericin treated CTL or *Plscr3*$^{-/-}$ J774 were mixed with 5 x 10^5 WT J774 in 50 μl PBS and then subcutaneously injected into the flanks of mice. Tumor growth was monitored by measuring tumor long (L) and short (W) diameters every other day. Tumor volume was calculated according to the equation: volume = 0.5 x L x W^2.

FISH
iBMDMs grown on poly-L-lysine-coated coverslips were treated as indicated and then fixed with 4% PFA for 10 min at room temperature, followed by permeabilization with 100% methanol for 10 min at -20°C. After three washes with 2x SSC buffer, coverslips were covered with a drop of hybridization buffer (10% dextran sulfate, 35% formamide, 30 mM sodium citrate, 0.3 M NaCl, 20 mM DTT) supplemented with 300 nM poly(A) probe (Cy3-dT_{50}) or 1 μM *18S* rRNA probe (Cy5-GGA CCA GAG CGA AAG CAT TTG CC). Coverslips were then incubated sequentially in 65°C for 5 min, 45°C for 30 min, and 42°C for 90 min before washing with 2x SSC for at least three times at 37°C and staining with DAPI in 2x SSC for 5 min. Images were captured using an Olympus Fluoview FV1000 Confocal System and fluorescence intensity was measured using ImageJ.

qRT-PCR

RNA extracted using TRIzol Reagent was reverse transcribed using the PrimeScript™ RT Master Mix (Takara, RR036A) according to the manufacturer's protocol. Real-time fluorescent quantitative PCR was performed using the Power SYBRGreen PCR Master Mix (Applied Biosystems, 1711564) and a QuantStudio™ 12K Flex (ThermoFisher).

Quantification and statistical analysis

Standard deviation (SD) and standard error of the mean (SEM) were calculated as indicated in each figure legend. Student's *t* test (2-tailed, unpaired) was used to determine differences between two groups. One- or two-way ANOVA was used to calculate differences among multiple groups. Differences between SYTOX green/PI uptake curves were compared by first calculating the area-under-the-curve values for each sample and then comparing different groups using the Student's *t*-test or one-way ANOVA. Type I errors were corrected by the Holm-Sidak method. *P* values <0.05 were considered significant.

References:

1. Liu, X., and Lieberman, J. (2017). A Mechanistic Understanding of Pyroptosis: The Fiery Death Triggered by Invasive Infection. Adv Immunol *135*, 81-117. 10.1016/bs.ai.2017.02.002.
2. Zanoni, I., Tan, Y., Di Gioia, M., Broggi, A., Ruan, J., Shi, J., Donado, C.A., Shao, F., Wu, H., Springstead, J.R., and Kagan, J.C. (2016). An endogenous caspase-11 ligand elicits interleukin-1 release from living dendritic cells. Science *352*, 1232-1236. 10.1126/science.aaf3036.
3. Shi, J., Zhao, Y., Wang, K., Shi, X., Wang, Y., Huang, H., Zhuang, Y., Cai, T., Wang, F., and Shao, F. (2015). Cleavage of GSDMD by inflammatory caspases determines pyroptotic cell death. Nature *526*, 660-665. 10.1038/nature15514.
4. Kayagaki, N., Stowe, I.B., Lee, B.L., O'Rourke, K., Anderson, K., Warming, S., Cuellar, T., Haley, B., Roose-Girma, M., Phung, Q.T., et al. (2015). Caspase-11 cleaves gasdermin D for non-canonical inflammasome signalling. Nature *526*, 666-671. 10.1038/nature15541.
5. Liu, X., Zhang, Z., Ruan, J., Pan, Y., Magupalli, V.G., Wu, H., and Lieberman, J. (2016). Inflammasome-activated gasdermin D causes pyroptosis by forming membrane pores. Nature *535*, 153-158. 10.1038/nature18629.
6. Ding, J., Wang, K., Liu, W., She, Y., Sun, Q., Shi, J., Sun, H., Wang, D.C., and Shao, F. (2016). Pore-forming activity and structural autoinhibition of the gasdermin family. Nature *535*, 111-116. 10.1038/nature18590.
7. Aglietti, R.A., Estevez, A., Gupta, A., Ramirez, M.G., Liu, P.S., Kayagaki, N., Ciferri, C., Dixit, V.M., and Dueber, E.C. (2016). GsdmD p30 elicited by caspase-11 during pyroptosis forms pores in membranes. Proc Natl Acad Sci U S A *113*, 7858-7863. 10.1073/pnas.1607769113.
8. Xia, S., Zhang, Z., Magupalli, V.G., Pablo, J.L., Dong, Y., Vora, S.M., Wang, L., Fu, T.M., Jacobson, M.P., Greka, A., et al. (2021). Gasdermin D pore structure reveals preferential release of mature interleukin-1. Nature *593*, 607-611. 10.1038/s41586-021-03478-3.
9. Liu, X., Xia, S., Zhang, Z., Wu, H., and Lieberman, J. (2021). Channelling inflammation: gasdermins in physiology and disease. Nat Rev Drug Discov *20*, 384-405. 10.1038/s41573-021-00154-z.
10. Lieberman, J., Wu, H., and Kagan, J.C. (2019). Gasdermin D activity in inflammation and host defense. Sci Immunol *4*, eaav1447. 10.1126/sciimmunol.aav1447.
11. Evavold, C.L., Ruan, J., Tan, Y., Xia, S., Wu, H., and Kagan, J.C. (2018). The Pore-Forming Protein Gasdermin D Regulates Interleukin-1 Secretion from Living Macrophages. Immunity *48*, 35-44 e36. 10.1016/j.immuni.2017.11.013.
12. Kroemer, G., Galluzzi, L., and Brenner, C. (2007). Mitochondrial membrane permeabilization in cell death. Physiol Rev *87*, 99-163. 10.1152/physrev.00013.2006.
13. Pfanner, N., Warscheid, B., and Wiedemann, N. (2019). Mitochondrial proteins: from biogenesis to functional networks. Nat Rev Mol Cell Biol *20*, 267-284. 10.1038/s41580-018-0092-0.
14. Mehta, M.M., Weinberg, S.E., and Chandel, N.S. (2017). Mitochondrial control of immunity: beyond ATP. Nat Rev Immunol *17*, 608-620. 10.1038/nri.2017.66.
15. Taylor, R.C., Cullen, S.P., and Martin, S.J. (2008). Apoptosis: controlled demolition at the cellular level. Nat Rev Mol Cell Biol *9*, 231-241. 10.1038/nrm2312.
16. Green, D.R., and Kroemer, G. (2004). The pathophysiology of mitochondrial cell death. Science *305*, 626-629. 10.1126/science.1099320.
17. Bonora, M., Giorgi, C., and Pinton, P. (2022). Molecular mechanisms and consequences of mitochondrial permeability transition. Nat Rev Mol Cell Biol *23*, 266-285. 10.1038/s41580-021-00433-y.

18. Bock, F.J., and Tait, S.W.G. (2020). Mitochondria as multifaceted regulators of cell death. Nat Rev Mol Cell Biol *21*, 85-100. 10.1038/s41580-019-0173-8.
19. Martinvalet, D., Dykxhoorn, D.M., Ferrini, R., and Lieberman, J. (2008). Granzyme A cleaves a mitochondrial complex I protein to initiate caspase-independent cell death. Cell *133*, 681-692. 10.1016/j.cell.2008.03.032.
20. Jacquemin, G., Margiotta, D., Kasahara, A., Bassoy, E.Y., Walch, M., Thiery, J., Lieberman, J., and Martinvalet, D. (2015). Granzyme B-induced mitochondrial ROS are required for apoptosis. Cell Death Differ *22*, 862-874. 10.1038/cdd.2014.180.
21. de Vasconcelos, N.M., Van Opdenbosch, N., Van Gorp, H., Parthoens, E., and Lamkanfi, M. (2019). Single-cell analysis of pyroptosis dynamics reveals conserved GSDMD-mediated subcellular events that precede plasma membrane rupture. Cell Death Differ *26*, 146-161. 10.1038/s41418-018-0106-7.
22. Rogers, C., Erkes, D.A., Nardone, A., Aplin, A.E., Fernandes-Alnemri, T., and Alnemri, E.S. (2019). Gasdermin pores permeabilize mitochondria to augment caspase-3 activation during apoptosis and inflammasome activation. Nat Commun *10*, 1689. 10.1038/s41467-019-09397-2.
23. Huang, L.S., Hong, Z., Wu, W., Xiong, S., Zhong, M., Gao, X., Rehman, J., and Malik, A.B. (2020). mtDNA Activates cGAS Signaling and Suppresses the YAP-Mediated Endothelial Cell Proliferation Program to Promote Inflammatory Injury. Immunity *52*, 475-486 e475. 10.1016/j.immuni.2020.02.002.
24. Platnich, J.M., Chung, H., Lau, A., Sandall, C.F., Bondzi-Simpson, A., Chen, H.M., Komada, T., Trotman-Grant, A.C., Brandelli, J.R., Chun, J., et al. (2018). Shiga Toxin/Lipopolysaccharide Activates Caspase-4 and Gasdermin D to Trigger Mitochondrial Reactive Oxygen Species Upstream of the NLRP3 Inflammasome. Cell Rep *25*, 1525-1536 e1527. 10.1016/j.celrep.2018.09.071.
25. Yu, J., Nagasu, H., Murakami, T., Hoang, H., Broderick, L., Hoffman, H.M., and Horng, T. (2014). Inflammasome activation leads to Caspase-1-dependent mitochondrial damage and block of mitophagy. Proc Natl Acad Sci U S A *111*, 15514-15519. 10.1073/pnas.1414859111.
26. de Torre-Minguela, C., Gomez, A.I., Couillin, I., and Pelegrin, P. (2021). Gasdermins mediate cellular release of mitochondrial DNA during pyroptosis and apoptosis. FASEB J *35*, e21757. 10.1096/fj.202100085R.
27. Zhou, R., Yazdi, A.S., Menu, P., and Tschopp, J. (2011). A role for mitochondria in NLRP3 inflammasome activation. Nature *469*, 221-225. 10.1038/nature09663.
28. Evavold, C.L., Hafner-Bratkovic, I., Devant, P., D'Andrea, J.M., Ngwa, E.M., Borsic, E., Doench, J.G., LaFleur, M.W., Sharpe, A.H., Thiagarajah, J.R., and Kagan, J.C. (2021). Control of gasdermin D oligomerization and pyroptosis by the Ragulator-Rag-mTORC1 pathway. Cell *184*, 4495-4511 e4419. 10.1016/j.cell.2021.06.028.
29. Chu, C.T., Ji, J., Dagda, R.K., Jiang, J.F., Tyurina, Y.Y., Kapralov, A.A., Tyurin, V.A., Yanamala, N., Shrivastava, I.H., Mohammadyani, D., et al. (2013). Cardiolipin externalization to the outer mitochondrial membrane acts as an elimination signal for mitophagy in neuronal cells. Nat Cell Biol *15*, 1197-1205. 10.1038/ncb2837.
30. de Kroon, A.I., Dolis, D., Mayer, A., Lill, R., and de Kruijff, B. (1997). Phospholipid composition of highly purified mitochondrial outer membranes of rat liver and Neurospora crassa. Is cardiolipin present in the mitochondrial outer membrane? Biochimica et Biophysica Acta *1325*, 108-116.
31. Chen, D., Zhang, X.Y., and Shi, Y. (2006). Identification and functional characterization of hCLS1, a human cardiolipin synthase localized in mitochondria. Biochem J *398*, 169-176. 10.1042/BJ20060303.

32. Liu, J., Dai, Q., Chen, J., Durrant, D., Freeman, A., Liu, T., Grossman, D., and Lee, R.M. (2003). Phospholipid Scramblase 3 Controls Mitochondrial Structure, Function, and Apoptotic Response. Mol Cancer Res *1*, 892-902.
33. Pizzuto, M., and Pelegrin, P. (2020). Cardiolipin in Immune Signaling and Cell Death. Trends Cell Biol *30*, 892-903. 10.1016/j.tcb.2020.09.004.
34. Liu, X., Fu, R., Pan, Y., Meza-Sosa, K.F., Zhang, Z., and Lieberman, J. (2018). PNPT1 Release from Mitochondria during Apoptosis Triggers Decay of Poly(A) RNAs. Cell *174*, 187-201 e112. 10.1016/j.cell.2018.04.017.
35. Di Gioia, M., Spreafico, R., Springstead, J.R., Mendelson, M.M., Joehanes, R., Levy, D., and Zanoni, I. (2020). Endogenous oxidized phospholipids reprogram cellular metabolism and boost hyperinflammation. Nat Immunol *21*, 42-53. 10.1038/s41590-019-0539-2.
36. Jung, J., Zeng, H., and Horng, T. (2019). Metabolism as a guiding force for immunity. Nat Cell Biol *21*, 85-93. 10.1038/s41556-018-0217-x.
37. Dang, E.V., McDonald, J.G., Russell, D.W., and Cyster, J.G. (2017). Oxysterol Restraint of Cholesterol Synthesis Prevents AIM2 Inflammasome Activation. Cell *171*, 1057-1071 e1011. 10.1016/j.cell.2017.09.029.
38. Desjardins, P., Frost, E., and Morais, R. (1985). Ethidium bromide-induced loss of mitochondrial DNA from primary chicken embryo fibroblasts. Mol Cell Biol *5*, 1163-1169. 10.1128/mcb.5.5.1163-1169.1985.
39. Steinhorn, B., Sorrentino, A., Badole, S., Bogdanova, Y., Belousov, V., and Michel, T. (2018). Chemogenetic generation of hydrogen peroxide in the heart induces severe cardiac dysfunction. Nat Commun *9*, 4044. 10.1038/s41467-018-06533-2.
40. Saeedi Saravi, S.S., Eroglu, E., Waldeck-Weiermair, M., Sorrentino, A., Steinhorn, B., Belousov, V., and Michel, T. (2020). Differential endothelial signaling responses elicited by chemogenetic H2O2 synthesis. Redox Biol *36*, 101605. 10.1016/j.redox.2020.101605.
41. Pak, V.V., Ezerina, D., Lyublinskaya, O.G., Pedre, B., Tyurin-Kuzmin, P.A., Mishina, N.M., Thauvin, M., Young, D., Wahni, K., Martinez Gache, S.A., et al. (2020). Ultrasensitive Genetically Encoded Indicator for Hydrogen Peroxide Identifies Roles for the Oxidant in Cell Migration and Mitochondrial Function. Cell Metab *31*, 642-653 e646. 10.1016/j.cmet.2020.02.003.
42. Devant, P., Borsic, E., Ngwa, E.M., Xiao, H., Chouchani, E.T., Thiagarajah, J.R., Hafner-Bratkovic, I., Evavold, C.L., and Kagan, J.C. (2023). Gasdermin D pore-forming activity is redox-sensitive. Cell Rep *42*, 112008. 10.1016/j.celrep.2023.112008.
43. Mukhopadhyay, P., Rajesh, M., Hasko, G., Hawkins, B.J., Madesh, M., and Pacher, P. (2007). Simultaneous detection of apoptosis and mitochondrial superoxide production in live cells by flow cytometry and confocal microscopy. Nat Protoc *2*, 2295-2301. 10.1038/nprot.2007.327.
44. Hu, J.J., Liu, X., Xia, S., Zhang, Z., Zhang, Y., Zhao, J., Ruan, J., Luo, X., Lou, X., Bai, Y., et al. (2020). FDA-approved disulfiram inhibits pyroptosis by blocking gasdermin D pore formation. Nat Immunol *21*, 736-745. 10.1038/s41590-020-0669-6.
45. Rathkey, J.K., Benson, B.L., Chirieleison, S.M., Yang, J., Xiao, T.S., Dubyak, G.R., Huang, A.Y., and Abbott, D.W. (2017). Live-cell visualization of gasdermin D-driven pyroptotic cell death. J Biol Chem *292*, 14649-14658. 10.1074/jbc.M117.797217.
46. He, W.T., Wan, H., Hu, L., Chen, P., Wang, X., Huang, Z., Yang, Z.H., Zhong, C.Q., and Han, J. (2015). Gasdermin D is an executor of pyroptosis and required for interleukin-1beta secretion. Cell Res *25*, 1285-1298. 10.1038/cr.2015.139.
47. Zhang, Z., Zhang, Y., Xia, S., Kong, Q., Li, S., Liu, X., Junqueira, C., Meza-Sosa, K.F., Mok, T.M.Y., Ansara, J., et al. (2020). Gasdermin E suppresses tumour growth by activating anti-tumour immunity. Nature *579*, 415-420. 10.1038/s41586-020-2071-9.

48. Wang, Q., Wang, Y., Ding, J., Wang, C., Zhou, X., Gao, W., Huang, H., Shao, F., and Liu, Z. (2020). A bioorthogonal system reveals antitumour immune function of pyroptosis. Nature *579*, 421-426. 10.1038/s41586-020-2079-1.
49. Merrick, B.A., Dhungana, S., Williams, J.G., Aloor, J.J., Peddada, S., Tomer, K.B., and Fessler, M.B. (2011). Proteomic profiling of S-acylated macrophage proteins identifies a role for palmitoylation in mitochondrial targeting of phospholipid scramblase 3. Mol Cell Proteomics *10*, M110 006007. 10.1074/mcp.M110.006007.
50. Katayama, K., Sakurai, I., and Wada, H. (2004). Identification of an Arabidopsis thaliana gene for cardiolipin synthase located in mitochondria. FEBS Lett *577*, 193-198. 10.1016/j.febslet.2004.10.009.
51. Sorice, M., Circella, A., Misasi, R., Pittoni, V., Garofalo, T., Cirelli, A., Pavan, A., Pontieri, G., and Valesini, G. (2000). Cardiolipin on the surface of apoptotic cells as a possible trigger for antiphospholipid antibodies. Clinical Experimental Immunology *122*, 277-284.
52. Thomas, M.P., Liu, X., Whangbo, J., McCrossan, G., Sanborn, K.B., Basar, E., Walch, M., and Lieberman, J. (2015). Apoptosis Triggers Specific, Rapid, and Global mRNA Decay with 3' Uridylated Intermediates Degraded by DIS3L2. Cell Rep *11*, 1079-1089. 10.1016/j.celrep.2015.04.026.
53. Kondolf, H.C., D'Orlando, D.A., Dubyak, G.R., and Abbott, D.W. (2023). Protein engineering reveals that gasdermin A preferentially targets mitochondrial membranes over the plasma membrane during pyroptosis. J Biol Chem *299*, 102908. 10.1016/j.jbc.2023.102908.
54. Neel, D.V., Basu, H., Gunner, G., Bergstresser, M.D., Giadone, R.M., Chung, H., Miao, R., Chou, V., Brody, E., Jiang, X., et al. (2023). Gasdermin-E mediates mitochondrial damage in axons and neurodegeneration. Neuron *111*, 1222-1240. e1229.
55. Iyer, S.S., He, Q., Janczy, J.R., Elliott, E.I., Zhong, Z., Olivier, A.K., Sadler, J.J., Knepper-Adrian, V., Han, R., Qiao, L., et al. (2013). Mitochondrial cardiolipin is required for Nlrp3 inflammasome activation. Immunity *39*, 311-323.
56. Schroder, K., and Tschopp, J. (2010). The inflammasomes. Cell *140*, 821-832. 10.1016/j.cell.2010.01.040.
57. Balasubramanian, A., Ghimire, L., Hsu, A.Y., Kambara, H., Liu, X., Hasegawa, T., Xu, R., Tahir, M., Yu, H., Lieberman, J., and Luo, H.R. (2023). Palmitoylation of gasdermin D directs its membrane translocation and pore formation in pyroptosis. bioRxiv. 10.1101/2023.02.21.529402.
58. Du, G., Healy, L.B., David, L., Walker, C., Fontana, P., Dong, Y., Devant, P., Puthenveetil, R., Ficarro, S.B., Banerjee, A., et al. (2023). ROS-dependent palmitoylation is an obligate licensing modification for GSDMD pore formation. bioRxiv. 10.1101/2023.03.07.531538.
59. Lutter, M., Fang, M., Luo, X., Nishijima, M., Xie, X., and Wang, X. (2000). Cardiolipin provides specificity for targeting of tBid to mitochondria. Nat Cell Biol *2*, 754-761. 10.1038/35036395.
60. Kuwana, T., Mackey, M.R., Perkins, G., Ellisman, M.H., Latterich, M., Schneiter, R., Green, D.R., and Newmeyer, D.D. (2002). Bid, Bax, and lipids cooperate to form supramolecular openings in the outer mitochondrial membrane. Cell *111*, 331-342. 10.1016/s0092-8674(02)01036-x.
61. Nomura, K., Imai, H., Koumura, T., Kobayashi, T., and Nakagawa, Y. (2000). Mitochondrial phospholipid hydroperoxide glutathione peroxidase inhibits the release of cytochrome c from mitochondria by suppressing the peroxidation of cardiolipin in hypoglycaemia-induced apoptosis. Biochem J *351*, 183-193. 10.1042/0264-6021:3510183.

62. Leventis, P.A., and Grinstein, S. (2010). The distribution and function of phosphatidylserine in cellular membranes. Annu Rev Biophys *39*, 407-427. 10.1146/annurev.biophys.093008.131234.
63. Tan, X., Thapa, N., Choi, S., and Anderson, R.A. (2015). Emerging roles of PtdIns(4, 5)P2–beyond the plasma membrane. J Cell Sci *128*, 4047-4056.
64. Zheng, Z., Deng, W., Bai, Y., Miao, R., Mei, S., Zhang, Z., Pan, Y., Wang, Y., Min, R., Deng, F., et al. (2021). The lysosomal Rag-Ragulator complex licenses RIPK1–and caspase-8–mediated pyroptosis by Yersinia. Science *372*, eabg0269.
65. McArthur, K., Whitehead, L.W., Heddleston, J.M., Li, L., Padman, B.S., Oorschot, V., Geoghegan, N.D., Chappaz, S., Davidson, S., San Chin, H., et al. (2018). BAK/BAX macropores facilitate mitochondrial herniation and mtDNA efflux during apoptosis. Science *359*. 10.1126/science.aao6047.
66. Wang, Y., Gao, W., Shi, X., Ding, J., Liu, W., He, H., Wang, K., and Shao, F. (2017). Chemotherapy drugs induce pyroptosis through caspase-3 cleavage of a gasdermin. Nature *547*, 99-103. 10.1038/nature22393.
67. Orning, P., Weng, D., Starheim, K., Ratner, D., Best, Z., Lee, B., Brooks, A., Xia, S., Wu, H., Kelliher, M.A., et al. (2018). Pathogen blockade of TAK1 triggers caspase-8-dependent cleavage of gasdermin D and cell death. Science *362*, 1064-1069. 10.1126/science.aau2818.
68. Sollberger, G., Choidas, A., Burn, G.L., Habenberger, P., Di Lucrezia, R., Kordes, S., Menninger, S., Eickhoff, J., Nussbaumer, P., Klebl, B., et al. (2018). Gasdermin D plays a vital role in the generation of neutrophil extracellular traps. Sci Immunol *3*, eaar6689. 10.1126/sciimmunol.aar6689.
69. Sarhan, J., Liu, B.C., Muendlein, H.I., Li, P., Nilson, R., Tang, A.Y., Rongvaux, A., Bunnell, S.C., Shao, F., Green, D.R., and Poltorak, A. (2018). Caspase-8 induces cleavage of gasdermin D to elicit pyroptosis during Yersinia infection. Proc Natl Acad Sci U S A *115*, E10888-E10897. 10.1073/pnas.1809548115.
70. Xia, S., Ruan, J., and Wu, H. (2019). Monitoring gasdermin pore formation in vitro. Methods Enzymol *625*, 95-107. 10.1016/bs.mie.2019.04.024.
71. Sanjana, N.E., Shalem, O., and Zhang, F. (2014). Improved vectors and genome-wide libraries for CRISPR screening. Nat Methods *11*, 783-784. 10.1038/nmeth.3047.

Key resources table

REAGENT or RESOURCE	SOURCE	IDENTIFIER
Antibodies		
Rabbit monoclonal anti-cleaved caspase-1 (Asp297)	Cell Signaling Technology	Cat# 4199; RRID: AB_1903916
Mouse monoclonal anti-GSDMD	This paper	N/A
Goat polyclonal anti-IL-1 beta	R&D systems	Cat# AF-201-NA; RRID: AB_354387
Mouse monoclonal anti-Cytochrome *c*	BioLegend	Cat# 612504; RRID: AB_2292697
Rabbit monoclonal anti-ACO2	Cell Signaling Technology	Cat# 6571; RRID: AB_2797630
Rabbit polyclonal anti-Caspase-3	Cell Signaling Technology	Cat# 9662; RRID: AB_331439
Rabbit monoclonal anti-COX IV	Cell Signaling Technology	Cat# 4850; RRID: AB_2085424
Mouse monoclonal anti-alpha-Tubulin	Sigma	Cat# T5168; RRID: AB_477579
Rabbit monoclonal anti-AIM2	Cell Signaling Technology	Cat# 53491
Rabbit polyclonal anti-SOD2	Santa Cruz Biotechnology	Cat# sc-30080; RRID: AB_661470
Rabbit monoclonal anti-HtrA2/Omi	Cell Signaling Technology	Cat# 9745; RRID: AB_11220423
Mouse monoclonal anti-caspase-1(p20)	Adipogen	Cat#AG-20B-0042-C100
Rat monoclonal anti-caspase-11	Cell Signaling Technology	Cat#14340S; RRID: AB_2728693
Human anti-Cardiolipin serum	USBiological	Cat# C1375
Mouse monoclonal anti-Actin	Sigma	Cat# A1978; RRID: AB_476692
Rabbit monoclonal anti-PLSCR3	Abcam	Cat# ab137128
Rabbit polyclonal anti-CRLS1	Abclonal	Cat# A12388; RRID: AB_2759232
Rabbit monoclonal anti-GSDMD	Abcam	Cat# ab209845; RRID: AB_2783550
Rabbit monoclonal anti-GSDMD	Abcam	Cat# ab219800; RRID: AB_2888940
Rabbit polyclonal anti-PNPT1	Proteintech	Cat# 14487-1-AP; RRID: AB_2165820
Rabbit monoclonal anti-Cytochrome C	Cell Signaling Technology	Cat# 4280; RRID: AB_10695410
Rabbit polyclonal anti-Tubulin	Cell Signaling Technology	Cat# 2148
Rabbit recombinant anti-HA-Tag	Cell Signaling Technology	Cat# 3724S; RRID: AB_1549585
Rabbit polyclonal anti-ASC	Adipogen	Cat#AG-25B-0006TS-C100; RRID: AB_2490440
Goat polyclonal anti-IL-1 beta	R&D systems	Cat# AF-201-NA; RRID: AB_354387
Rabbit monoclonal anti-LAMP1	Abcam	Cat# ab208943; RRID: AB_2923327

Anti-EEA1	Cell Signaling Technology	Cat# 3288
Anti-Calnexin	Cell Signaling Technology	Cat# 2679; RRID: AB_2228381
Mouse monoclonal anti-Lamin B1	Santa Cruz Biotechnology	Cat# sc-56144, RRID: AB_784272
Bacterial and Virus Strains		
Salmonella typhimurium	This paper	N/A
Chemicals, Peptides, and Recombinant Proteins		
Phorbol 12-myristate 13-acetate (PMA)	Sigma	Cat# P1585
E. coli LPS	InvivoGen	Cat# tlrl-pb5lps
Nigericin	InvivoGen	Cat# tlrl-Nig-5
MitoTracker Deep Red FM	Invitrogen	Cat# M22426
Image-iT™ TMRM Reagent	Invitrogen	Cat# I34361
MitoTracker green FM	Invitrogen	Cat# M7514
SYTOX™ Green Nucleic Acid Stain	Invitrogen	Cat# S7020
SYTOX™ Deep Red Nucleic Acid Stain	Invitrogen	Cat# S11381
4% PFA (paraformaldehyde)	Invitrogen	Cat# R37814
25% Glutaraldehyde	Sigma	Cat# 354400
Nunc Lab-Tek Chamber Slides	Thermo Scientific	Cat# 177402
35 mm Dish, 10 mm Glass Diameter	MatTek	Cat# P35G-1.5-10-C
Polyvinyl alcohol mounting medium with DABCO®, antifading	Sigma	Cat# 10981
Oligomycin	Sigma	Cat# 75351
FCCP	Sigma	Cat# C2920
Rotenone	Sigma	Cat# R8875
SuperSignal™ West Femto Maximum Sensitivity Substrate	Thermo Scientific	Cat# 34095
ATP solution	Thermo Scientific	Cat# R0441
MitoSOX™ Red Mitochondrial Superoxide Indicator	Invitrogen	Cat# M36008
MitoTracker Orange	Invitrogen	Cat# M7510
DAPI (4′,6-diamidino-2-phenylindole)	Invitrogen	Cat# D1306
Ethidium bromide solution	Sigma	Cat# E1510
MitoTEMPO	Sigma	Cat# SML0737
Poly(deoxyadenylic-thymidylic) acid sodium salt	Sigma	Cat# P0883
Ultrapure LPS	Sigma	Cat# LPS25
D-Alanine	Sigma	Cat# A7377
L-Alanine	Sigma	Cat# A7627
Propidium iodide	Invitrogen	Cat# P3566
Recombinant human GSDMD	Hao Wu Lab	N/A
Recombinant human caspase-11	Hao Wu Lab	N/A
Recombinant t-BID	Prospecbio	Cat# PRO-644
β-Nicotinamide adenine dinucleotide, reduced disodium salt hydrate (NADH)	Sigma	Cat# N8129
Z-VAD-FMK	BD Biosciences	Cat# 550377
Antimycin A from *Streptomyces* sp.	Sigma	Cat# A8674
Disulfiram	Sigma	Cat# 1224008
TRIzol™ Reagent	Invitrogen	Cat# 15596026
MCC950	Sigma	Cat# 5381200001
N-Ethylmaleimide	Cayman	Cat# 19938

VBIT-4	Invivochem	Cat# V2258
Cyclosporin A	Cayman	Cat# 12088
Bongkrekic Acid (ammonium salt)	Cayman	Cat# 19079
Mitomycin C	Sigma	Cat# M5353
Nonyl Acridine Orange	Sigma	Cat# A7847
Piericidin A	Aladdin	Cat# P329435
2-Thenoyltrifluoroacetone	MedChemExpress	Cat# HY-D0190
Recombinant Murine TNF-a	PeproTech	Cat# 315-01A
Etoposide	Sigma	Cat# E1383
CHX	Aladdin	Cat# C112766
z-VAD-FMK	R&D systems	Cat# FMK001
Critical Commercial Assays		
Seahorse XFe96 FluxPaks	Agilent	Cat# 102416-100
DNeasy Blood & Tissue Kit	Qiagen	Cat# 69506
SsoFast EvaGreen Supermix	Bio-Rad	Cat# 1725205
Amaxa Mouse Macrophage Nucleofection Kit	Lonza	Cat# VPA-1009
DCFDA/H2DCFDA Cellular ROS Assay	Abcam	Cat# ab113851
JC-1 Mitochondrial Membrane Potential Assay	Abcam	Cat# ab113850
MitoProbe™ DiIC1(5) Assay	Invitrogen	Cat# M34151
CytoTox 96 ® Non-Radioactive Cytotoxicity Assay	Promega	Cat# G1780
CellTiter-Glo® Luminescent Cell Viability Assay	Promega	Cat# G7570
X-tremeGENE™ HP DNA Transfection Reagent	Roche	Cat# 6366236001
SYBRGreen PCR Master Mix	Applied Biosystems	Cat# 1711564
PrimeScript™ RT Master Mix	Takara	Cat# RR036A
Mouse IL-1 beta/IL-1F2 Quantikine ELISA Kit	R&D systems	Cat# MLB00C
Experimental models: Cell lines		
Human: THP-1	ATCC	Cat# TIB-202; RRID: CVCL_0006
Mouse: immortalized BMDMs	This Paper	N/A
Human: HEK293T	ATCC	Cat# CRL-3216; RRID: CVCL_0063
Human: HCT116	ATCC	Cat# CCL-247; RRID: CVCL_0291
Mouse: J774	ATCC	Cat# TIB-67; RRID: CVCL_4692
Experimental models: Organisms/strains		
Mouse: BALB/cJ	The Jackson Laboratory	Cat#: 000651; RRID: IMSR_JAX: 000651
Oligonucleotides		
Human mtDNA F: GACGTTAGGTCAAGGTGTAG Human mtDNA R: CAACTAAGCACTCTACTCTC	Integrated DNA Technologies	N/A
Human GAPDH F: GACCCCTTCATTGACCTCAAC Human GAPDH R: CTTCTCCATGGTGGTGAAGA	Integrated DNA Technologies	N/A
Mouse Actb F: GTGACGTTGACATCCGTAAAGA Mouse Actb R: GCCGGACTCATCGTACTCC	Integrated DNA Technologies	N/A
Mouse Sdha F: TCCTACCCGATCACATACTGTT Mouse Sdha R: GCTCTGTCATGTAATGGATGGCA	Integrated DNA Technologies	N/A
Mouse Tuba F: GGAGGGGACGACTCCTTCA Mouse Tuba R: TGGGCCATTTCGGATCTCATC	Integrated DNA Technologies	N/A

Mouse 7SL F: GCACTAAGTTCGGCATCAATATG Mouse 7SL R: CTGATCAGCACGGGAGTTT	Tsingke Biological Technology	N/A
Mouse U6 F: CTCGCTTCGGCAGCACA Mouse U6 R: AACGCTTCACGAATTTGCGT	Tsingke Biological Technology	N/A
Mouse Plscr3 F: CGACGCGTATGGCAGGCTACTTGC Mouse Plscr3 R: GCGGATCCCTAACTGGTGATGGCA	Tsingke Biological Technology	N/A
Mouse Crls1 F: CGACGCGTGCCACCATGTTGGCTTGGCGCGT Mouse Crls1 R: TGCATGCATTCATTTGCCCTTTATCACCTGAACAGTT	Tsingke Biological Technology	N/A
Mouse Gapdh-F: GAAGGGCTCATGACCACAGT Mouse Gapdh-R: GGATGCAGGGATGATGTTCT	Tsingke Biological Technology	N/A
Mouse Tnfa-F: CCCTCACACTCAGATCATCTTCT Mouse Tnfa-R: GCTACGACGTGGGCTACAG	Tsingke Biological Technology	N/A
Mouse Il6-F: GAGAGGAGACTTCACAGAGGATAC Mouse Il6-R: GTACTCCAGAAGACCAGAGG	Tsingke Biological Technology	N/A
Mouse Il1b-F: GCAACTGTTCCTGAACTCAACT Mouse Il1b-R: ATCTTTTGGGGTCCGTCAACT	Tsingke Biological Technology	N/A
Recombinant DNA		
pLenti-CMV-Blast-HyPer7-DAAO-NES	This paper	N/A
pLenti-CMV-Blast-HyPer7-DAAO-NLS	This paper	N/A
pCMV-VSV-G	Addgene	Plasmid #8454; RRID: Addgene_8454
psPAX2	Addgene	Plasmid #12260; RRID: Addgene_12260
pFlag-CMV-mFL-GSDMD	(Liu et al., 2016)	N/A
pFlag-CMV-mNT-GSDMD	(Liu et al., 2016)	N/A
LentiCRISPR v2	Addgene	Plasmid #52961; RRID: Addgene_52961
Lenti-mNeonGreen-GSDMD	(Rathkey et al., 2017)	N/A
pHAGE-3X Flag-Plscr3	This paper	N/A
pHAGE-3X Flag-Plscr3 F259V	This paper	N/A
pHAGE-3X Flag-Plscr3 5A	This paper	N/A
pHAGE-3X Flag-Crls1	This paper	N/A
pHAGE-3X Flag-Crls1 D170A	This paper	N/A
pLenti-CMV-Puro-PNPT1	This paper	N/A
pLenti-CMV-Puro-PNPT1 S484A	This paper	N/A
pcDNA3-mGSDMD-NT-3x HA	This paper	N/A
pDsRed-hGSDMA-NT	This paper	N/A
pDsRed-mGSDME-NT	This paper	N/A
Software and algorithms		
Zeiss Zen software	Zeiss	N/A
Olympus Fluoview FV1000 Confocal System	Olympus	N/A
Prism 8.0	GraphPad Software	N/A
ImageJ	ImageJ	N/A
IDEAS 6.2 software	Luminex	N/A
FlowJo	FlowJo	N/A
Nikon Elements (v5.10)	Nikon	N/A

Fiji	ImageJ	N/A
Huygens Essential v19.10 (SVI)	Huygens	N/A
Arivis Vision4D	Arivis	N/A
BioRender	BioRender.com	N/A

Figure

Click here to access/download;Figure;Figure 1.tif

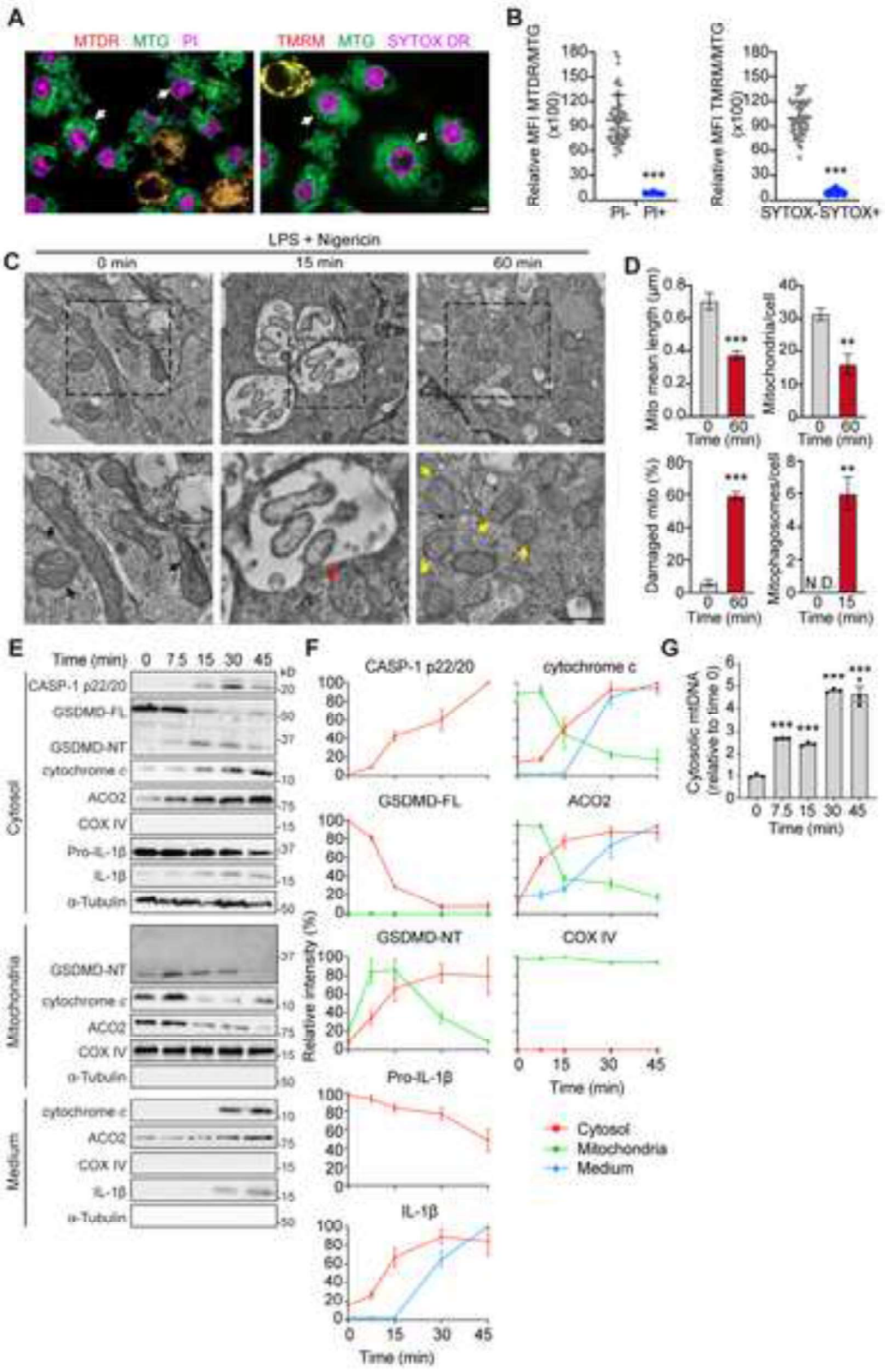

Figure 1

Figure

Click here to access/download;Figure;Figure 2.tif

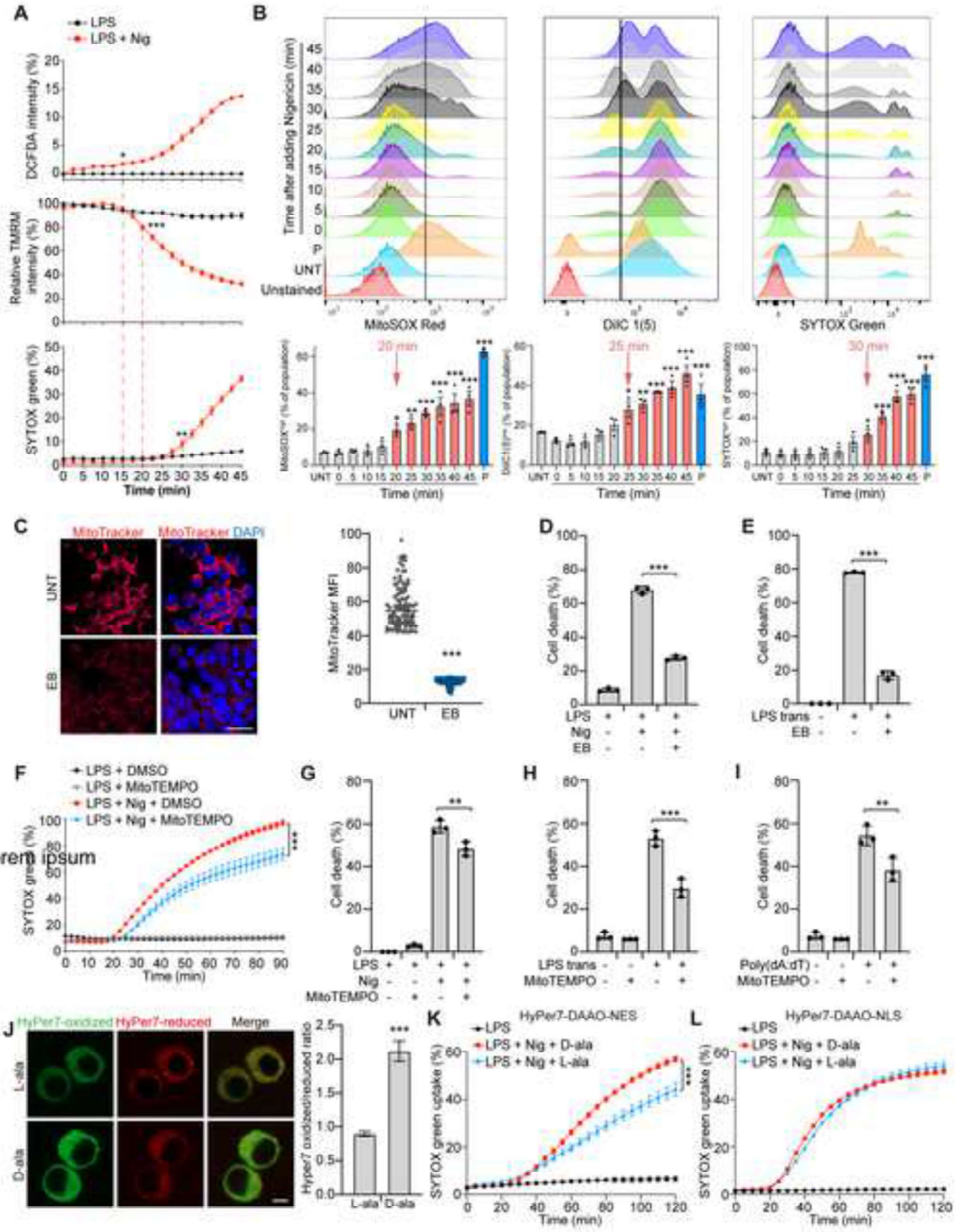

Figure 2

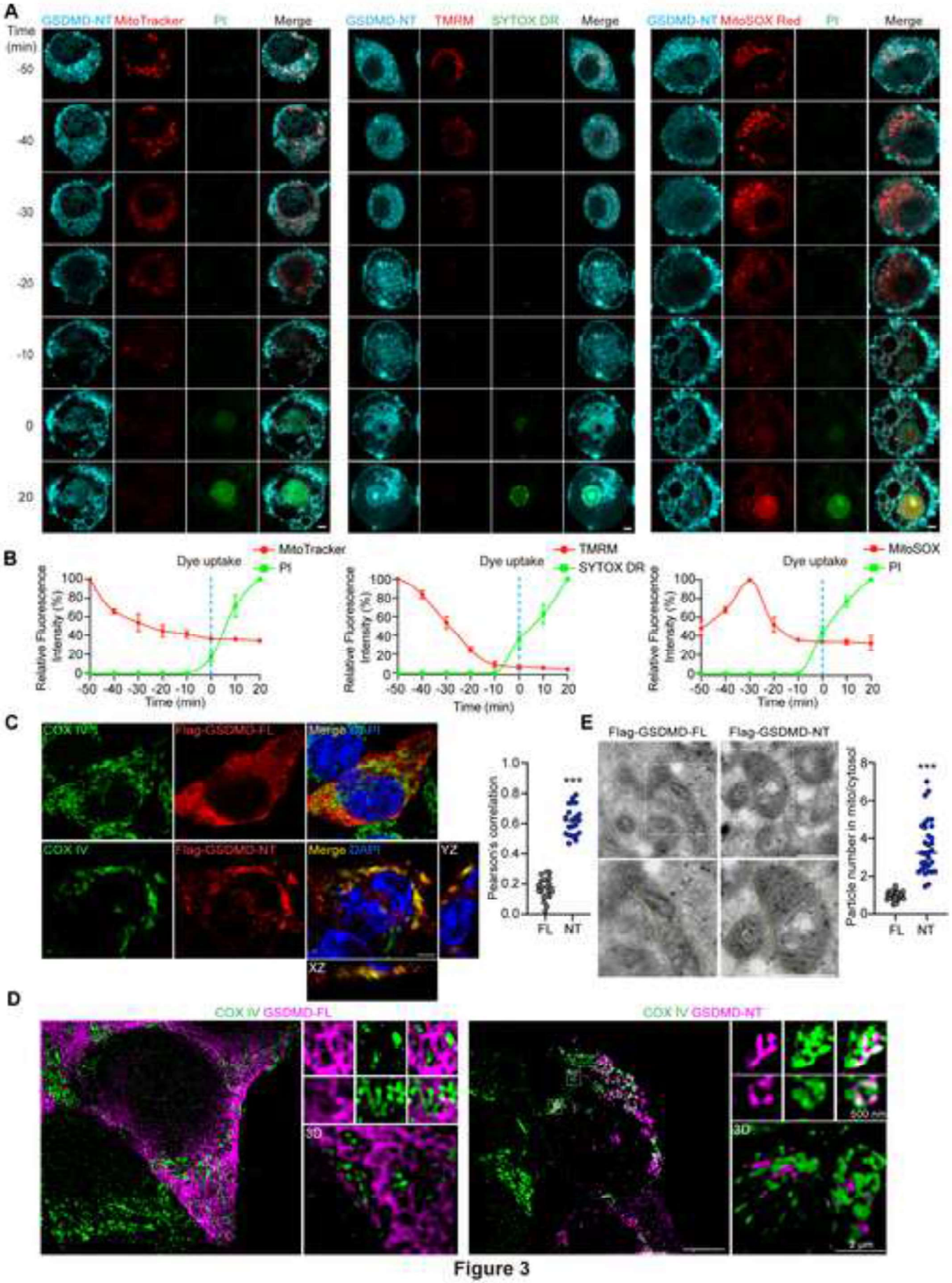

Figure 3

Figure

Click here to access/download;Figure;Figure 4.tif

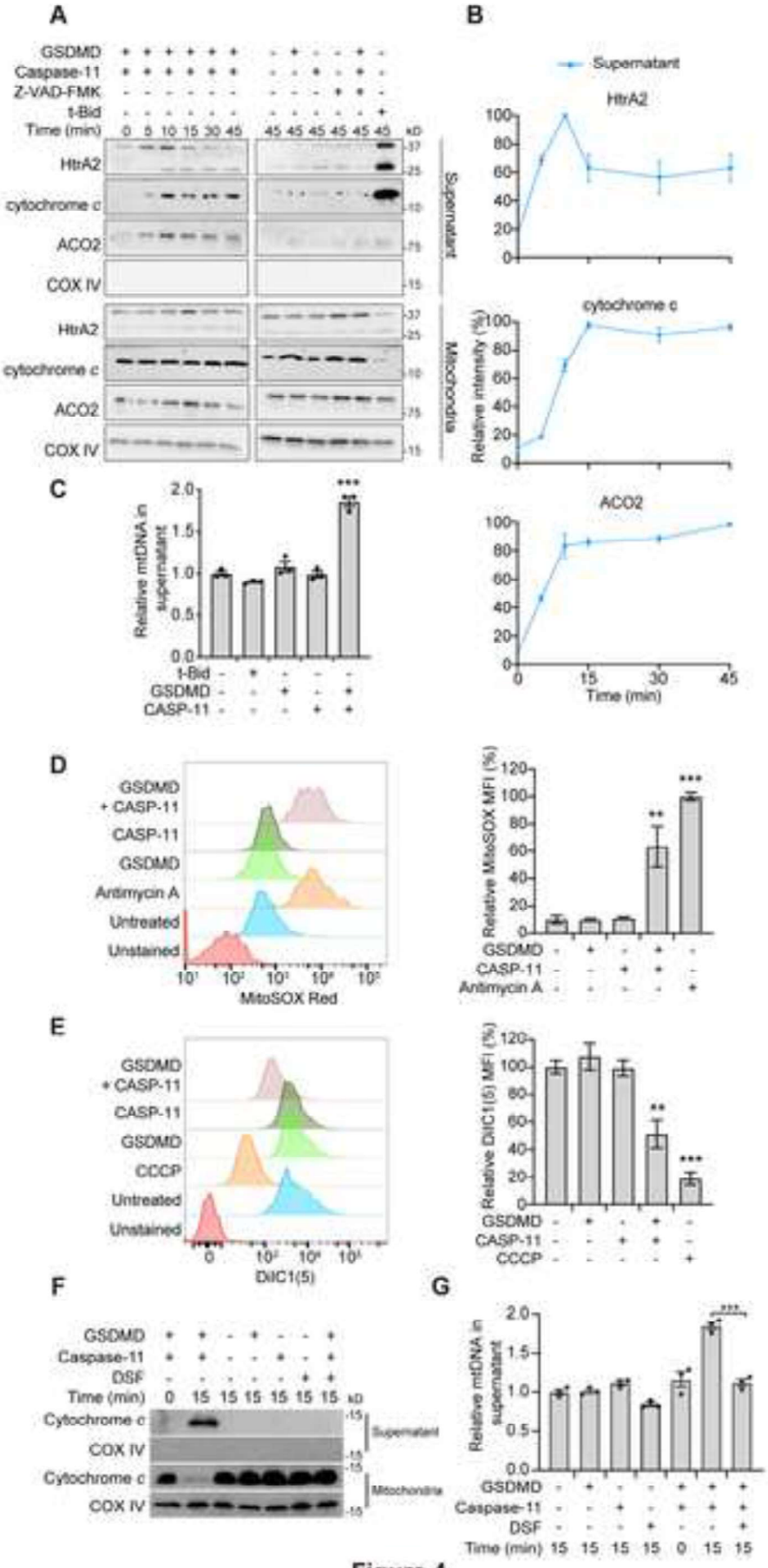

Figure 4

Figure

Click here to access/download;Figure;Figure 5.tif

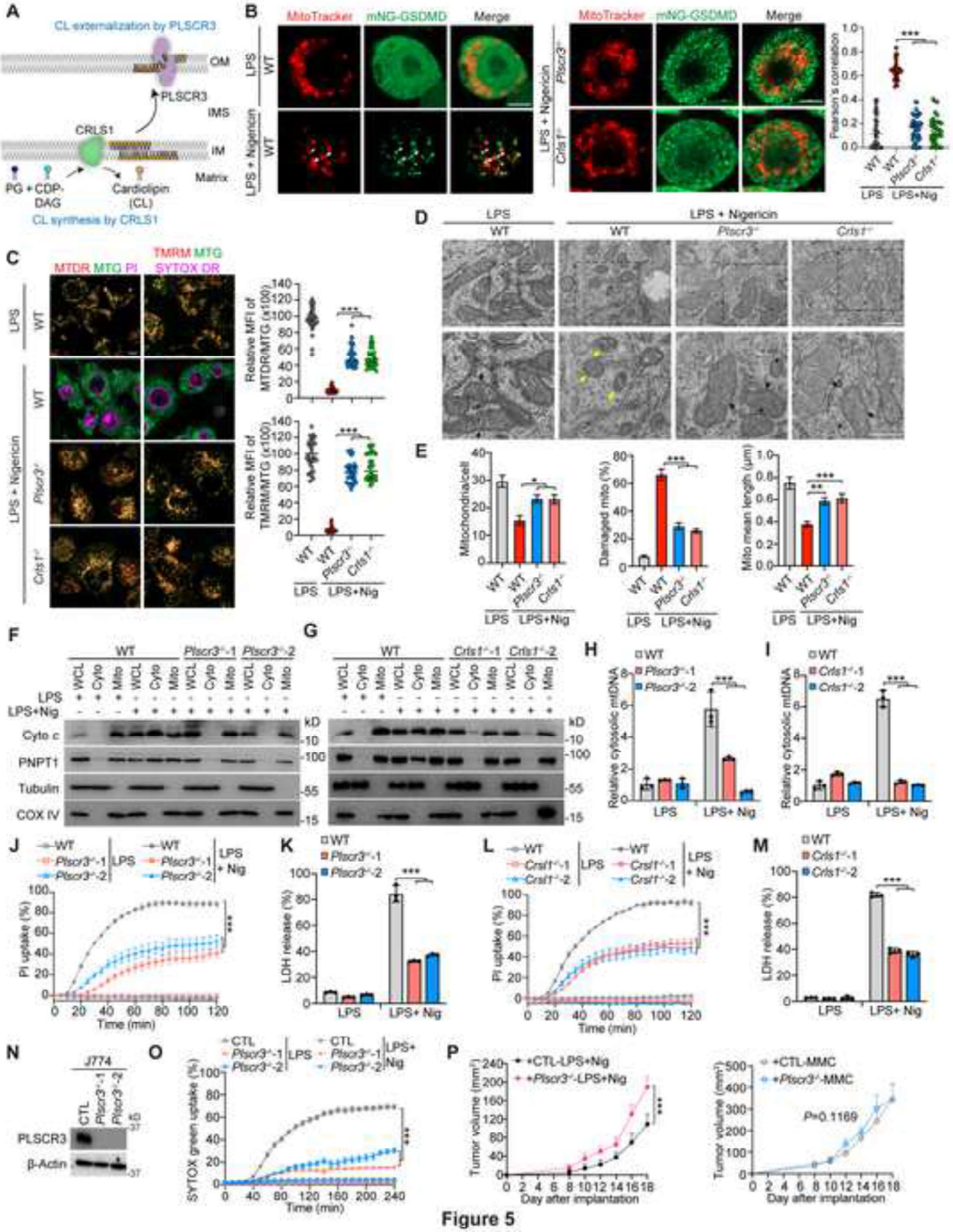

Figure 5

Figure

Click here to access/download;Figure;Figure 6.tif

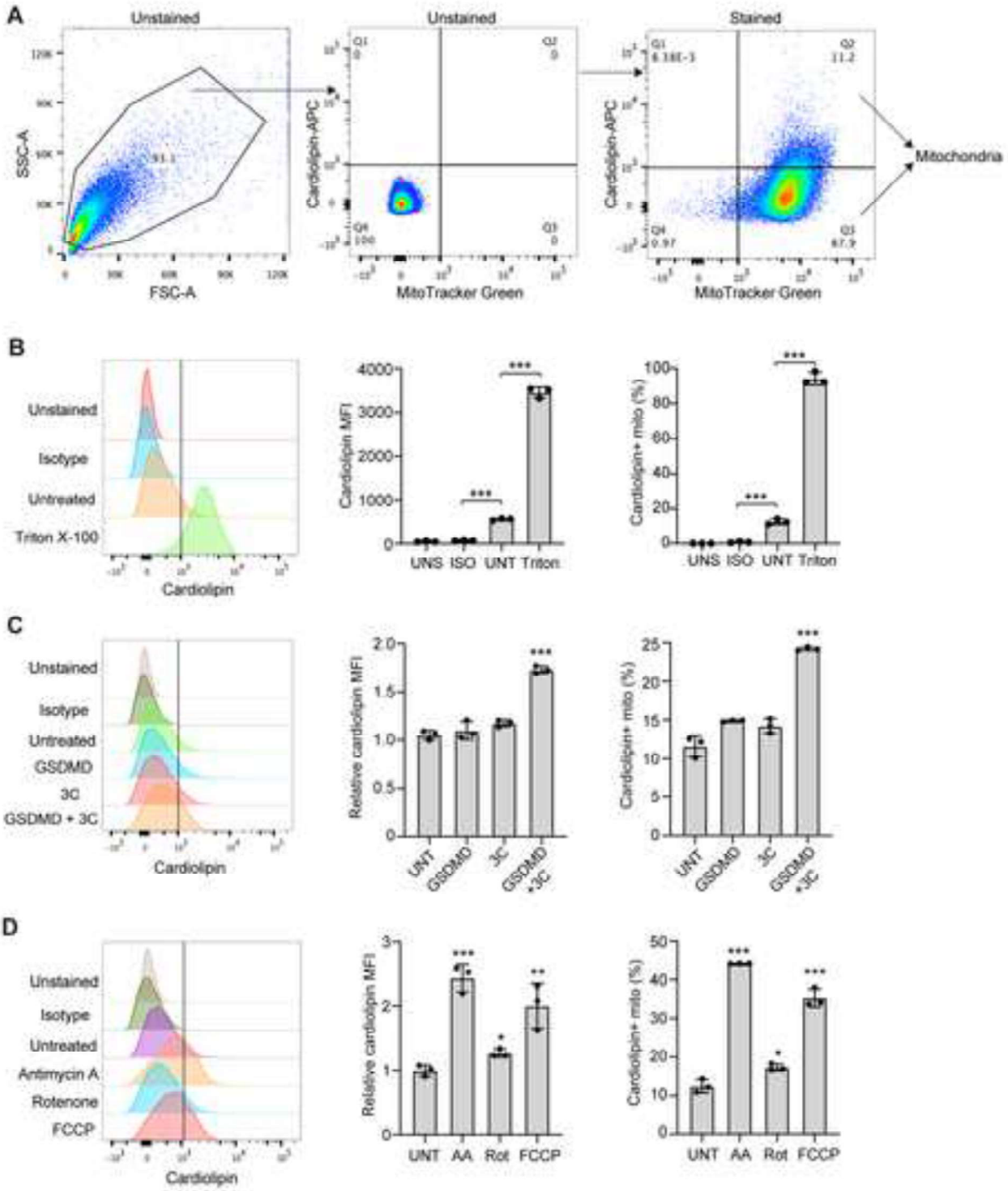

Figure 6

Figure

Click here to access/download;Figure;Figure 7.tif

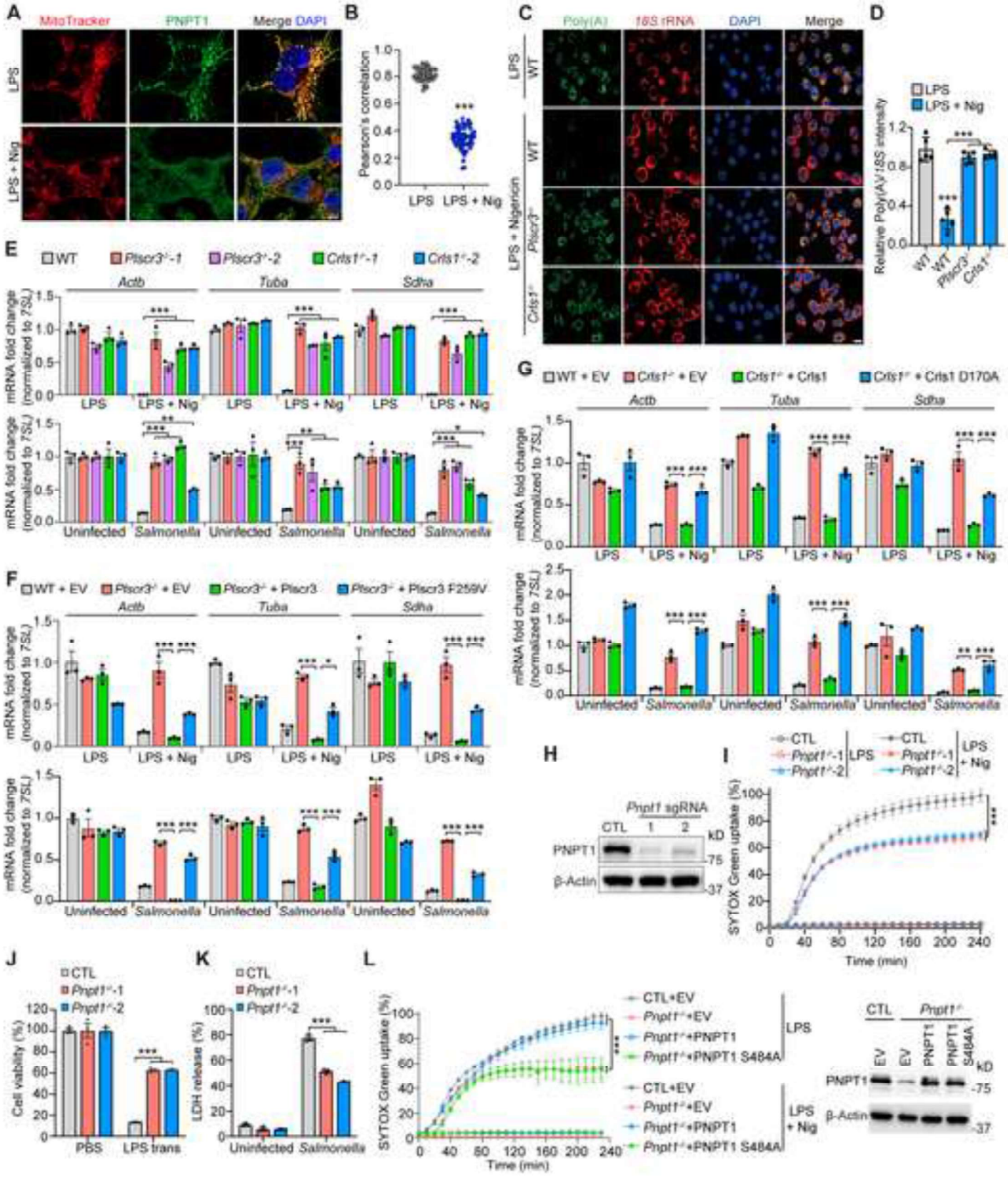

Figure 7